NONLINEAR LONGITUDINAL DYNAMICS OF AN ORBITAL LIFTING VEHICLE*

NGUYEN X. VINH

Dept. of Aerospace Engineering, The University of Michigan, Ann Arbor, Michigan 48104, U.S.A.

and

ARTHUR J. DOBRZELECKI

USAF, Air Force Weapons Laboratory, Kirtland Air Force Base, N.M., U.S.A.

(Received 9 June, 1969)

Abstract. This paper presents an analytical study of the longitudinal dynamics of a thrusting, lifting, orbital vehicle in a nearly circular orbit. The translational motion is composed of a nonlinear oscillation, or phugoid, and a spiral mode which results in either decay or dilatation of the orbit depending on the perturbed initial conditions. The nonlinear effects on the phugoid period and damping are small in the altitude range considered. Elements of the orbit such as radial distance, velocity, and flight path angle were obtained explicitly as functions of time. The behavior of the variations of these elements is correctly predicted. Explicit expressions for period and damping of the angle-of-attack mode were derived. It is shown that a critical altitude may exist at which the phugoid mode and the angle-of-attack mode have nearly equal periods. Near this resonance altitude linearized solutions are no longer valid and a study of the nonlinear equations shows that there is a strong interaction between the translational and the rotational modes resulting in a switching of the two frequencies of oscillations.

1. Introduction

In a report published in 1960, Etkin (1960) extended the classical theory of aircraft longitudinal flight dynamics to the hypersonic speed and orbital altitude regime. He investigated the perturbed motion of a lifting, thrusting vehicle, initially constrained to steady atmospheric flight along a great circle path, in the altitude range of 100 000–700 000 ft. By augmenting the classical low speed, low altitude equations of motion, to include the effects of Earth curvature and the atmospheric density and gravity gradients with respect to altitude, he obtained a fifth-order linear system of equations governing the motion of the vehicle. A numerical solution of the linearized equations showed that the motion contained two damped, oscillatory components which could be identified with the classical phugoid and short-period modes, and a new aperiodic spiral mode. Etkin further showed that the phugoid mode frequency could exceed that of the short-period mode at orbital altitudes. In a later paper, Etkin (1961) showed that gravity torques must be included in the equations of motion to correctly describe the short-period mode frequency at high altitudes.

In the same time period, Porter (1961) published a report in which he investigated the phugoid oscillations and spiral mode only. However, his analysis ranged from

* This work was supported by NASA Contract No. NASr 54(06).

Celestial Mechanics **3** (1971) 427–460.

low speeds to superorbital speeds, where the vehicle is constrained to a great circle flight path by negative lift. In the altitude range where they are comparable, Etkin's and Porter's results are in good agreement.

Also in the same time period, Rangi (1960) extended Etkin's results by including certain non-linear terms in the linearized equations and studying their effects on the perturbed vehicle motion on an analog computer. He found that the effects of the non-linear terms considered were negligible.

More recently, Laitone and Chou (1965) found analytical solutions to the linearized equations of motion that are in good agreement with Etkin's numerical results.

The above papers and the works of Morth and Speyer (1961) and Norman and Meier (1963), considered collectively, provide a comprehensive study of the longitudinal dynamics of a lifting, thrusting vehicle in the hypersonic speed and orbital altitude regimes. However, there remain gaps in the results previously obtained, specifically, an adequate analysis of non-linear effects and of the altitude region where the phugoid and short-period mode frequencies are nearly equal. It is the intent of the present study to fill these gaps and, in addition, to expand on the results previously obtained.

The example vehicle used for the numerical computations is the same as the one used by Etkin (1961). Its aerodynamic characteristics are given in the Appendix. They are typical of a future manned orbital, lifting vehicle, so that we may assume that the vehicle is ultimately controllable. For this reason we need only consider the perturbed vehicle motion for a time long enough to establish it mathematically. This time span will be, at most, the time the vehicle takes to orbit the Earth a few revolutions.

2. Preliminary Analysis

A. EQUATIONS OF MOTION

Consider the motion of a thrusting, lifting vehicle in a nearly circular orbit. Following Etkin (1961), we assume that the vehicle motion takes place about a nonrotating,

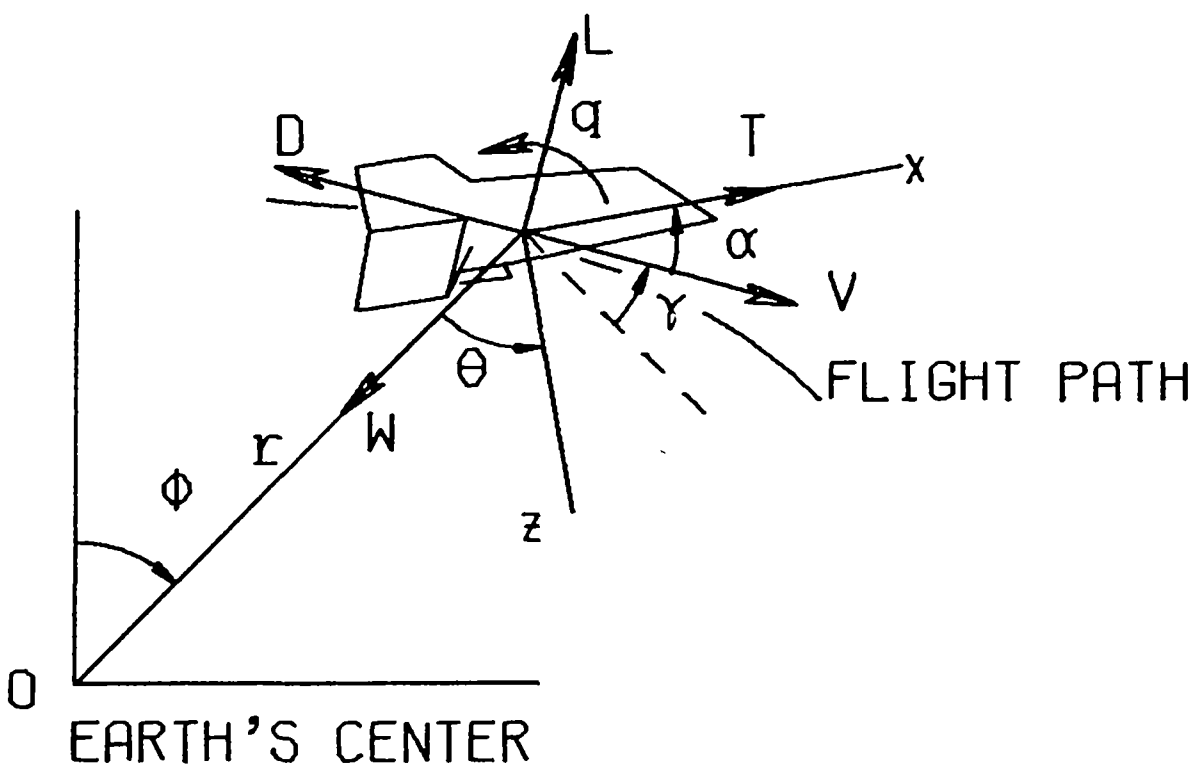

Fig. 1. Axis system and nomenclature.

spherical, homogeneous Earth, with a static atmosphere. Then, referred to a right-handed coordinate system, that is always tangent to the flight path as shown in Figure 1, the longitudinal motion of a lifting, thrusting vehicle is governed by the system of equations.*

$$\begin{aligned}
\frac{\mathrm{d}V}{\mathrm{d}t} &= \frac{T}{m}\cos\alpha - \frac{\varrho S C_D V^2}{2m} - g\sin\gamma \\
V\frac{\mathrm{d}\gamma}{\mathrm{d}t} &= \frac{T}{m}\sin\alpha + \frac{\varrho S C_L V^2}{2m} - \left(g - \frac{V^2}{r}\right)\cos\gamma \\
\frac{\mathrm{d}q}{\mathrm{d}t} &= \frac{\varrho S L C_m V^2}{2B} - \frac{3}{2}\frac{g}{r}\frac{(A-C)}{B}\sin 2\theta \\
\frac{\mathrm{d}\theta}{\mathrm{d}t} &= q + \frac{V}{r}\cos\gamma \\
\frac{\mathrm{d}r}{\mathrm{d}t} &= V\sin\gamma \\
\theta &= \gamma + \alpha\,.
\end{aligned} \tag{1}$$

The first term of the pitching moment equation is the familiar aerodynamic torque and is a restoring torque for aerodynamically stable vehicle configurations. The second term is the gravity torque and is, on the contrary, destabilizing for normal aircraft-like configurations. A complete discussion of gravity torques is given by Beletskii (1966) and Roberson (1958). At a sufficiently high altitude the gravity torque can become larger in absolute value than the aerodynamic torque.

The vehicle is assumed to be initially traveling along a great circle flight path of radius r_0. The circular flight is sustained by the constant thrust T. This value of the thrust is assumed constant during subsequent motion of the vehicle. Furthermore, the thrust is small enough (Etkin, 1960) that the mass of the vehicle (during the time span of a few revolutions) can be assumed constant also. By setting $\alpha=\gamma=0$ in Equation (1), we have along the reference orbit

$$\begin{aligned}
T &= \tfrac{1}{2}\varrho_0 S C_{D_0} u_0^2 \\
1 - \frac{u_0^2}{g_0 r_0} &= \frac{\varrho_0 S C_{L_0} u_0^2}{2 m g_0} \\
C_{m_0} &= 0 \\
q &= -\frac{u_0}{r_0}\,.
\end{aligned} \tag{2}$$

For flight in the hypersonic speed regime, the aerodynamic coefficients are independent of the Mach number (Laitone and Chou, 1965) but, generally, non-linear in

* All symbols are defined in notation section at end of paper.

other dependent variables (Donovan *et al.*, 1961). For small perturbations, we may assume

$$\begin{aligned} C_D(\alpha) &= C_{D_0} + C_{D_\alpha}\alpha \\ C_L(\alpha) &= C_{L_0} + C_{L_\alpha}\alpha \\ C_m(\alpha, q) &= C_{m_0} + C_{m_\alpha}\alpha + \frac{L}{2u_0} C_{m_{\hat{q}}}(q - q_0) \end{aligned} \tag{3}$$

where C_{D_0}, C_{L_0} and C_{m_0} are the drag, lift and pitching moment coefficients along the reference flight path.

B. NON-DIMENSIONAL EQUATIONS OF MOTION

To write the equations in non-dimensional forms, let

$$\begin{aligned} V(t) &= u_0\hat{u}(t), \qquad r(t) = r_0\hat{r}(t), \qquad q(t) = \frac{2u_0}{L}\hat{q}(t) \\ \varrho(r) &= \varrho_0\hat{\varrho}(r), \qquad g(r) = g_0\left(\frac{r_0}{r}\right)^2 = g_0\left(\frac{1}{\hat{r}}\right)^2 \end{aligned} \tag{4}$$

and define the quantities

$$\begin{aligned} \hat{t} &= \frac{g_0}{u_0}t, \qquad k_y^2 = \frac{B}{m}, \qquad \frac{\mathrm{d}}{\mathrm{d}\hat{t}}(\,) = (\dot{}) \\ \eta &= \frac{\varrho_0 S u_0^2}{2mg_0}, \qquad k_0 = \frac{(A - C)}{B}, \qquad l = \frac{2r_0}{L} \\ s^2 &= \frac{u_0^2}{g_0 r_0}, \qquad \delta = \left(\frac{L}{2k_y}\right)^2. \end{aligned} \tag{5}$$

Then Equation (1) can be written in the non-dimensional forms

$$\begin{aligned} \dot{\hat{u}} &= \eta C_{D_0}\cos\alpha - \eta\hat{\varrho}\hat{u}^2 C_D(\alpha) - \frac{1}{\hat{r}^2}\sin\gamma \\ \hat{u}\dot{\gamma} &= \eta C_{D_0}\sin\alpha + \eta\hat{\varrho}\hat{u}^2 C_L(\alpha) - \left(\frac{1}{\hat{r}^2} - \frac{s^2\hat{u}^2}{\hat{r}}\right)\cos\gamma \\ \dot{\hat{q}} &= 2\eta\delta\hat{\varrho}\hat{u}^2 C_m(\alpha, \hat{q}) - \frac{3k_0}{2l\hat{r}^3}\sin 2\theta \\ \dot{\theta} &= s^2 l\hat{q} + s^2\frac{\hat{u}}{\hat{r}}\cos\gamma \\ \dot{\hat{r}} &= s^2\hat{u}\sin\gamma \\ \theta &= \gamma + \alpha \end{aligned} \tag{6}$$

where the thrust has been replaced by its equivalent drag force from Equation (2).

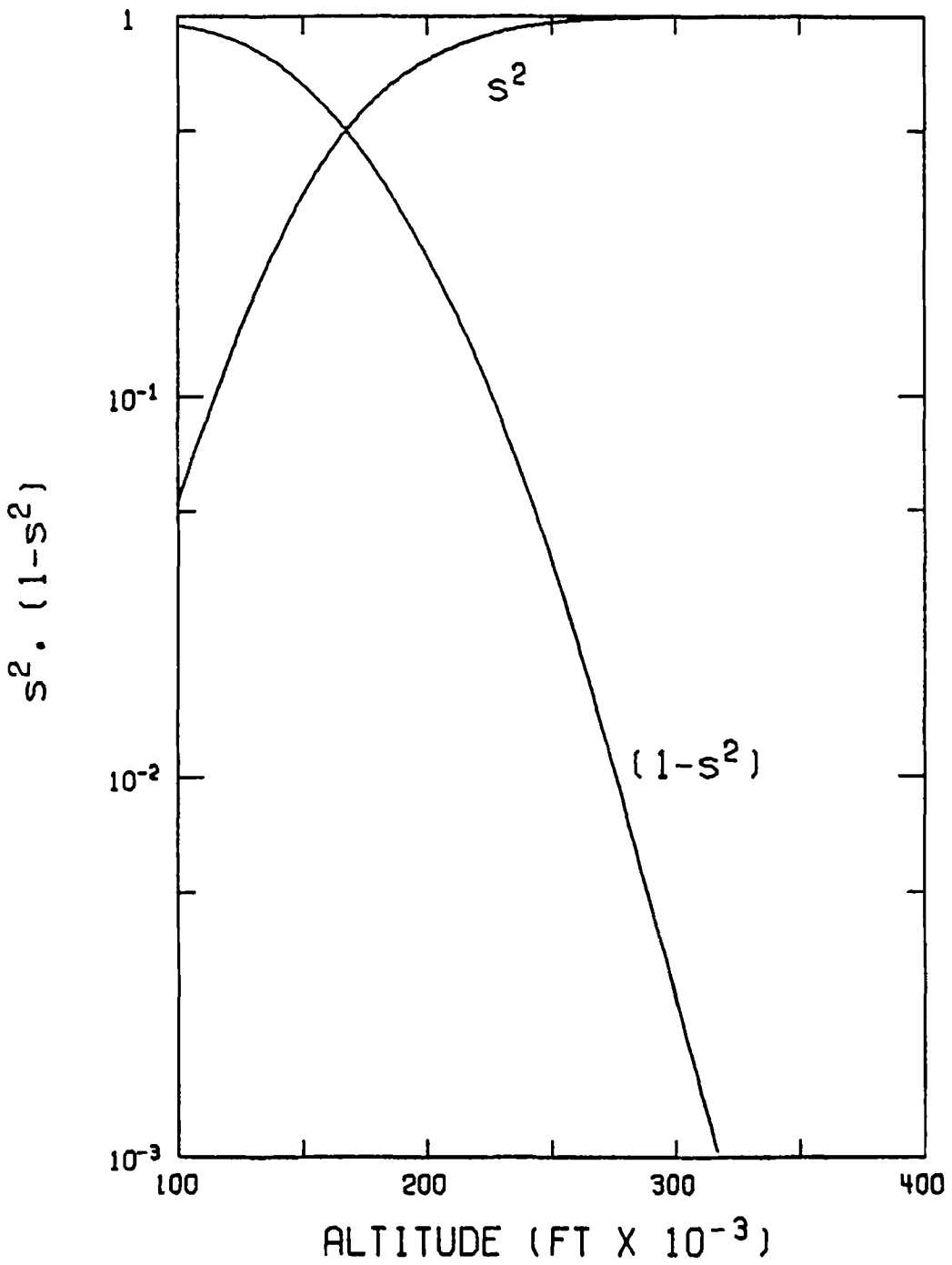

Fig. 2. Speed ratio, s^2.

The quantity s is the ratio of the vehicle speed along the reference flight path to the drag free circular orbital speed at a radius r_0. As shown in Figure 2, s is nearly unity above about 300000 ft altitude. The quantity η is the ratio of the dynamic pressure force over the reference area to the weight of the vehicle. It decreases rapidly with altitude as shown in Figure 3. As the altitude increases above that shown $\varrho \to 0$, hence $\eta \to 0$ also. These figures are plotted using Etkin's vehicle. The quantity l is directly proportional to the flight path radius and is of the order 8.5×10^5 for Etkin's vehicle (Etkin, 1961).

If we set $\eta = 0$ and $s^2 = 1$ in Equation (6) the equations reduce to the familiar drag free satellite equations. Then, changes in the rigid-body motion about the vehicle's center of mass have no effect on the vehicle trajectory. However, the converse is in general not true. This suggests a method that will be used in the analysis of the trajectory or phugoid mode, that is, we will decouple Equation (6) by assuming that motion about the vehicle center of mass has little effect on the trajectory of the vehicle. This assumption of the so-called limited problem has been used in celestial mechanics to study the libration of the Moon. Based on this decoupling, we shall first calculate the trajectory mode, and then use the results to integrate the equations governing the angle-of-attack oscillations. The coupling effects will be examined in the last part of the paper.

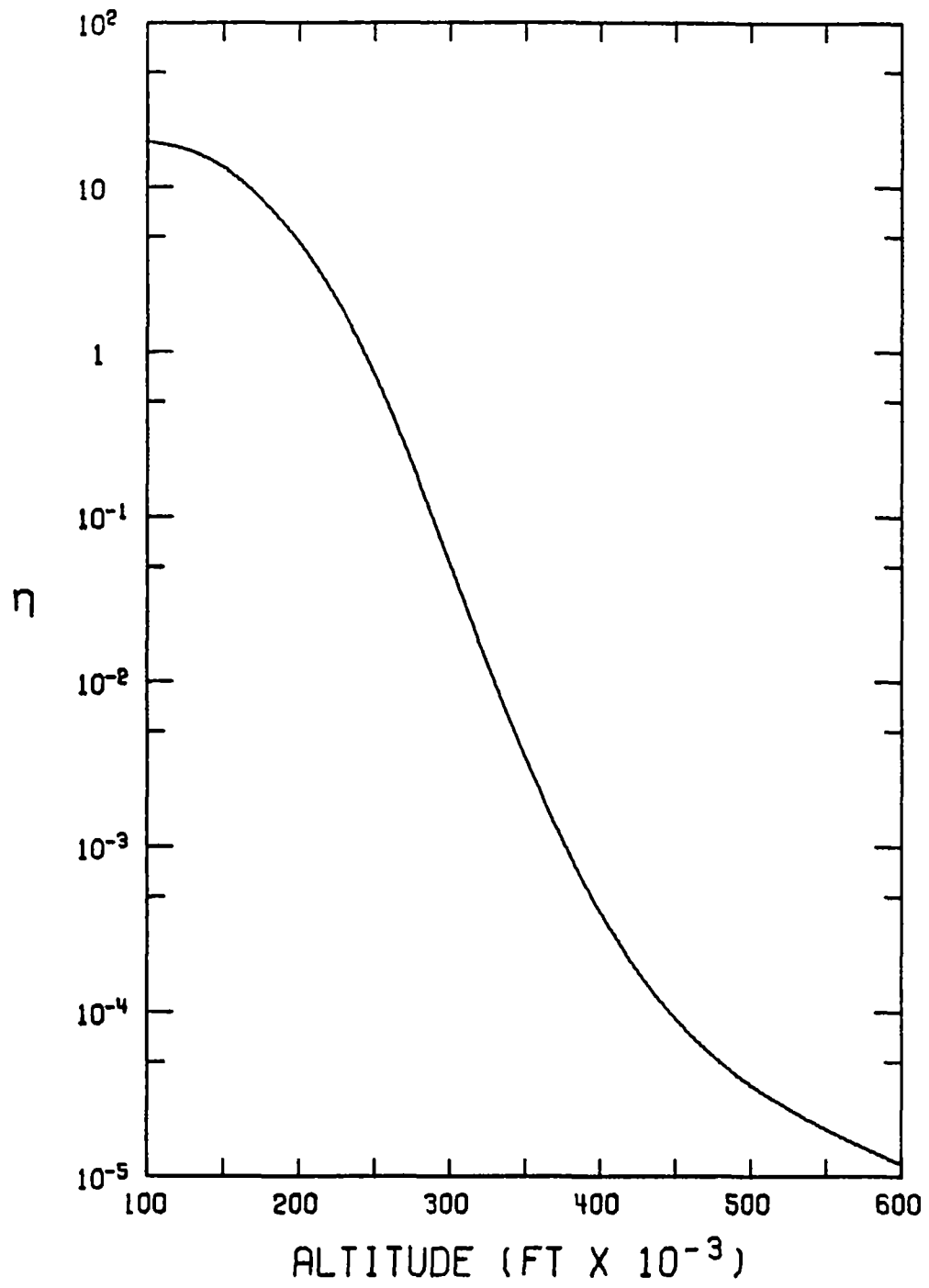

Fig. 3. Non-dimensional dynamic pressure force, η.

C. SMALL PERTURBATION EQUATIONS

We select the variables $\hat{u}$, γ, $\hat{r}$, $l\hat{q}$ and α to represent the state of the system. If we allow only small departures from the reference flight path, we can express these state variables in terms of small perturbations

$$\begin{aligned} \hat{u} &= 1 + \hat{u}_1 \\ \gamma &= \gamma_1 \\ \hat{r} &= 1 + \hat{r}_1 \\ l\hat{q} &= -1 + \hat{q}_1 \\ \alpha &= \alpha_1 \,. \end{aligned} \tag{7}$$

Also, by expanding the atmospheric density $\hat{\varrho}$ in a Taylor's series in $\hat{r}_1$, we have

$$\hat{\varrho}(\hat{r}_1) = 1 + \sigma_1 \hat{r}_1 + \sigma_2 \hat{r}_1^2 + \cdots \tag{8}$$

where

$$\sigma_1 = \left(\frac{\mathrm{d}\varrho}{\mathrm{d}r}\right)_0 \frac{r_0}{\varrho_0}, \qquad \sigma_2 = \frac{1}{2}\left(\frac{\mathrm{d}^2\varrho}{\mathrm{d}r^2}\right)_0 \frac{r_0^2}{\varrho_0}, \ldots . \tag{9}$$

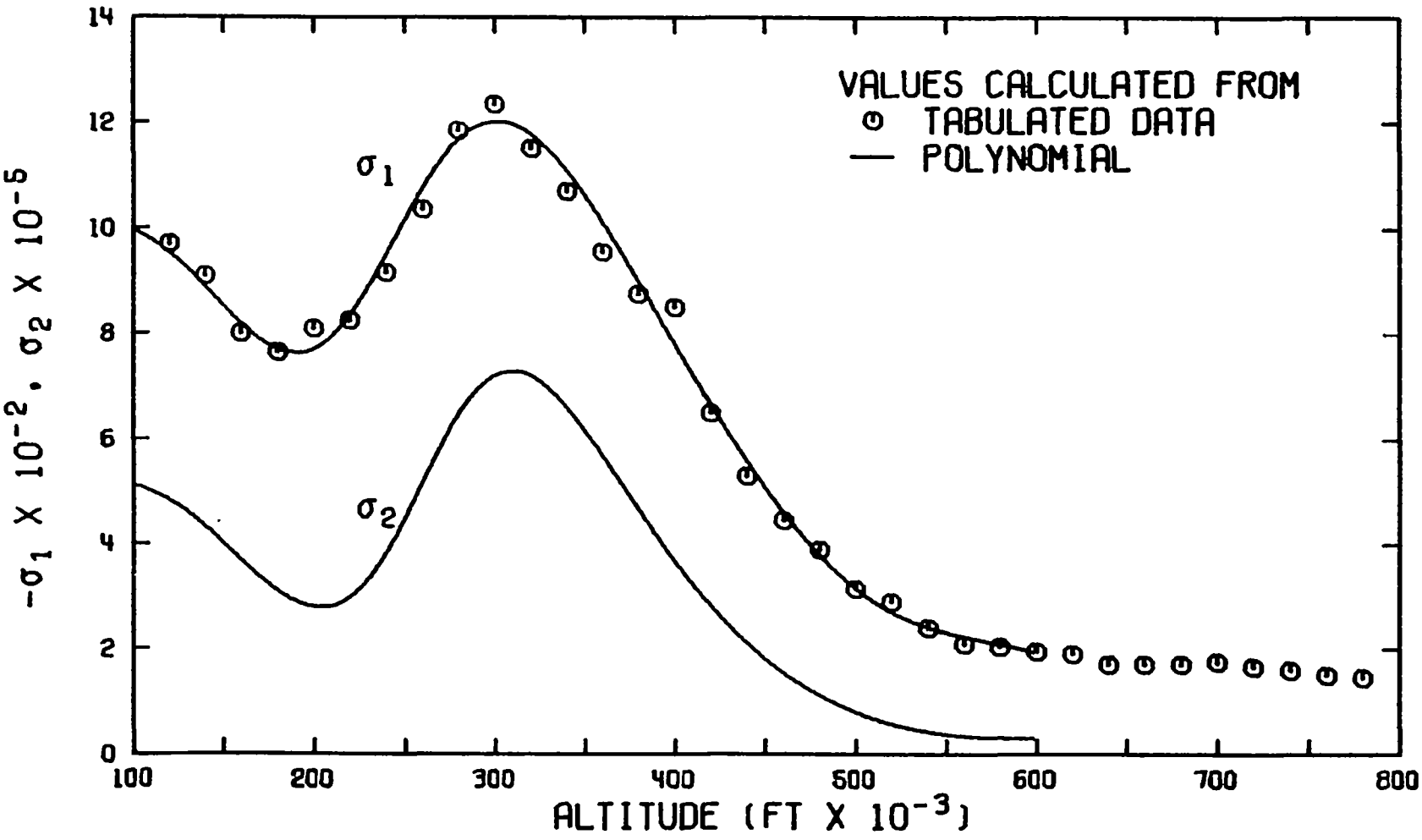

Fig. 4. Atmospheric mass density gradients.

For computational purposes the atmospheric data used were obtained from a polynomial representation of the 1962 U.S. standard atmosphere as presented in the 1966 U.S. standard atmosphere supplement. The variations of the atmospheric mass density gradients σ_1 and σ_2 as functions of the altitude are presented in Figure 4.

Further, let

$$\begin{aligned} \omega^2 &= (1 - s^2)(-\sigma_1 s^2 + 2) + s^4 \\ \beta &= -\tfrac{1}{2}s^2[(1 - s^2)(\sigma_2 - 1) - 2] \\ n^2 &= s^2[3k_0 - 2\eta\delta l C_{m_\alpha}] \\ C_{N_1} &= \tfrac{1}{2}[C_{D_0} + C_{L_\alpha} - 2\delta C_{m_{\hat{q}}}] \\ C_{N_2} &= \tfrac{1}{2}[C_{D_0} + C_{L_\alpha} + 2\delta C_{m_{\hat{q}}}] \end{aligned} \tag{10}$$

$$\tau = \omega\hat{t}, \qquad \frac{\mathrm{d}}{\mathrm{d}\tau}(\,) = (\,)'.$$

Using the relations 7, 8, and 10 in Equation (6), we have, to the second order of magnitude of smallness, the small perturbation equations

$$X' = AX + B(X) \tag{11}$$

where

$$X = \begin{bmatrix} \hat{u}_1 \\ \gamma_1 \\ \hat{r}_1 \\ \hat{q}_1 \\ \alpha_1 \end{bmatrix},$$

$$A = \frac{1}{\omega}\begin{bmatrix} -2\eta C_{D_0} & -1 & -\eta C_{D_0}\sigma_1 & 0 & -\eta C_{D_\alpha} \\ 2 & 0 & -\dfrac{(\omega^2-2)}{s^2} & 0 & \eta(C_{N_1}+C_{N_2}) \\ 0 & s^2 & 0 & 0 & 0 \\ 0 & -3k_0 & 0 & -\eta(C_{N_1}-C_{N_2}) & -\dfrac{n^2}{s^2} \\ -(2-s^2) & 0 & \dfrac{\omega^2-(2+s^2)}{s^2} & s^2 & -\eta(C_{N_1}+C_{N_2}) \end{bmatrix} \tag{12}$$

$$B(X) = \frac{1}{\omega}\begin{bmatrix} -\eta C_{D_0}(\hat{u}_1^2 + 2\sigma_1\hat{u}_1\hat{r}_1 + \sigma_2\hat{r}_1^2) + 2\gamma_1\hat{r}_1 - \eta C_{D_\alpha}\alpha_1(\sigma_1\hat{r}_1 + 2\hat{u}_1) - \eta C_{D_0}\dfrac{\alpha_1^2}{2} \\ -\hat{u}_1^2 + \frac{1}{2}(1-s^2)\gamma_1^2 - \dfrac{2\beta}{s^2}\hat{r}_1^2 - \dfrac{(\omega^2-2+4s^2)}{s^2}\hat{r}_1\hat{u}_1 \\ \qquad + \eta C_{L_\alpha}\sigma_1\alpha_1\hat{r}_1 - \eta(C_{D_0}-C_{L_\alpha})\alpha_1\hat{u}_1 \\ s^2\hat{u}_1\gamma_1 \\ 2\eta\delta(2\hat{u}_1 + \sigma_1\hat{r}_1)(C_{m_\alpha}l\alpha_1 + C_{m_{\hat{q}}}\hat{q}_1) + 9k_0\hat{r}_1(\gamma_1+\alpha_1) \\ \hat{u}_1^2 - \frac{1}{2}\gamma_1^2 + \dfrac{(2\beta+s^4)}{s^2}\hat{r}_1^2 + \dfrac{1}{s^2}(\omega^2-2+4s^2-s^4)\hat{r}_1\hat{u}_1 \\ \qquad + \eta(C_{D_0}-C_{L_\alpha})\alpha_1\hat{u}_1 - \eta C_{L_\alpha}\sigma_1\alpha_1\hat{r}_1 \end{bmatrix}$$

In theory, it is not difficult to integrate Equation (11) analytically. Let ε be an initial perturbation of any one of the state variables. We can then assume series solutions of the form

$$\begin{aligned} \hat{u}_1 &= \varepsilon\hat{u}_{11} + \varepsilon^2\hat{u}_{12} + \cdots \\ \gamma_1 &= \varepsilon\gamma_{11} + \varepsilon^2\gamma_{12} + \cdots \\ \hat{r}_1 &= \varepsilon\hat{r}_{11} + \varepsilon^2\hat{r}_{12} + \cdots \\ \hat{q}_1 &= \varepsilon\hat{q}_{11} + \varepsilon^2\hat{q}_{12} + \cdots \\ \alpha_1 &= \varepsilon\alpha_{11} + \varepsilon^2\alpha_{12} + \cdots \end{aligned} \tag{13}$$

or

$$X = \varepsilon X_1 + \varepsilon^2 X_2 + \cdots \tag{14}$$

where the definitions of the vectors X_1, X_2,... are clear from Equation (13). By substituting into Equation (11) and equating the coefficients of like powers of ε we have the system of matrix differential equations

$$\begin{aligned} X_1' &= AX_1 \\ X_2' &= AX_2 + B(X_1) \\ &\cdots . \end{aligned} \tag{15}$$

Since the matrix A is constant, we can immediately integrate the first of Equation (15) to get

$$X_1(\tau) = e^{A\tau} X_1^0 \tag{16}$$

where

$$X_1^0 = X_1(0) = \frac{1}{\varepsilon} X(0). \tag{17}$$

With this value of $X_1(\tau)$, we can express $B(X_1)$ as a function of τ only and then consider the second of Equation (15) as a linear matrix differential equation with a forcing term. By integrating, we have

$$X_2(\tau) = e^{A\tau} X_2(0) + \int_0^{\tau} e^{A(\tau - t)} B(t)\, \mathrm{d}t. \tag{18}$$

But, since $X_2(0) = 0$, we have

$$X_2(\tau) = \int_0^{\tau} e^{A(\tau - t)} B(t)\, \mathrm{d}t \tag{19}$$

and the solution to the second order of magnitude of smallness is

$$X(\tau) = \varepsilon e^{A\tau} X_1^0 + \varepsilon^2 \int_0^{\tau} e^{A(\tau - t)} B(t)\, \mathrm{d}t. \tag{20}$$

3. The Mode Shapes

To express the components of the 5-vector $X(\tau)$ in the solution, (Equation 20), explicitly in terms of the non-dimensional time τ, it is required to solve a quintic characteristic equation. In order to get explicit analytical expressions, we will decouple the two modes and calculate them separately. In the last part of this chapter an approximate factorization of the quintic equation will be given and the coupling effect and the nonlinear effect will be examined.

A. SPIRAL AND PHUGOID MODES

The phugoid, or long period, oscillation occurs at nearly constant angle-of-attack. Hence, setting $\alpha \cong 0$ in Equation (20) and neglecting the moment equation, we have for the phugoid mode

$$\bar{X}(\tau) = \varepsilon e^{A_1 \tau} \bar{X}_1^0 + \varepsilon^2 \int_0^{\tau} e^{A_1(\tau - t)} B_1(t)\, \mathrm{d}t \tag{21}$$

where

$$\bar{X}(\tau) = \begin{bmatrix} \hat{u}_1 \\ \gamma_1 \\ \hat{r}_1 \end{bmatrix}, \qquad A_1 = \frac{1}{\omega} \begin{bmatrix} -2\eta C_{D_0} & -1 & -\eta C_{D_0}\sigma_1 \\ 2 & 0 & \dfrac{2-\omega^2}{s^2} \\ 0 & s^2 & 0 \end{bmatrix}$$

$$B_1(\tau) = B_1(\bar{X}_1) = \frac{1}{\omega} \begin{bmatrix} -\eta C_{D_0}(\hat{u}_{11}^2 + 2\sigma_1 \hat{u}_{11}\hat{r}_{11} + \sigma_2 \hat{r}_{11}^2) \\ \qquad + 2\gamma_{11}\hat{r}_{11} \\ -\hat{u}_{11}^2 + \frac{1}{2}(1-s^2)\gamma_{11}^2 - \dfrac{2\beta}{s^2}\hat{r}_{11}^2 \\ \qquad -\dfrac{1}{s^2}(\omega^2 - 2 + 4s^2)\hat{r}_{11}\hat{u}_{11} \\ s^2 \hat{u}_{11}\gamma_{11} \end{bmatrix}. \tag{22}$$

If we consider only the linear term, the system has the characteristic equation

$$\lambda^3 + \frac{2\eta C_{D_0}}{\omega}\lambda^2 + \lambda - \frac{2\eta C_{D_0}}{\omega}\left(\frac{\xi}{\omega}\right)^2 = 0 \tag{23}$$

where

$$\xi^2 = s^2[-(1+\sigma_1)s^2 + 2] = -\omega^2 - \sigma_1 s^2 + 2. \tag{24}$$

In general, the characteristic equation has a pair of complex conjugate roots corresponding to the phugoid oscillations and a real root corresponding to the spiral mode. The last term of the characteristic equation induces the spiral mode and is a small quantity. Let

$$\lambda_{\text{spiral}} = \frac{2\eta C_{D_0}}{\omega}\left(\frac{\xi}{\omega}\right)^2 a \tag{25}$$

where a is a quantity to be determined. By substituting into Equation (23) we have

$$a = 1 - \left(\frac{2\eta C_{D_0}}{\omega}\right)^2 \left(\frac{\xi}{\omega}\right)^2 a^2 \left(1 + \left(\frac{\xi}{\omega}\right)^2 a\right). \tag{26}$$

Using Lagrange's expansion (Bellman, 1964) we have for the value of a

$$\begin{aligned} a = 1 &- \left(\frac{2\eta C_{D_0}}{\omega}\right)^2 \left(\frac{\xi}{\omega}\right)^2 \left(1 + \left(\frac{\xi}{\omega}\right)^2\right) + \left(\frac{2\eta C_{D_0}}{\omega}\right)^4 \left(\frac{\xi}{\omega}\right)^4 \\ &\times \left(1 + \left(\frac{\xi}{\omega}\right)^2\right)\left(2 + 3\left(\frac{\xi}{\omega}\right)^2\right) - \left(\frac{2\eta C_{D_0}}{\omega}\right)^6 \left(\frac{\xi}{\omega}\right)^6 \left(1 + \left(\frac{\xi}{\omega}\right)^2\right) \\ &\times \left(1 + 2\left(\frac{\xi}{\omega}\right)^2\right)\left(5 + 6\left(\frac{\xi}{\omega}\right)^2\right) + \cdots. \end{aligned} \tag{27}$$

Then by factorizing the cubic equation, Equation (23), we have for the phugoid mode

$$\lambda^2 + \frac{2\eta C_{D_0}}{\omega}\left(1 + \left(\frac{\xi}{\omega}\right)^2 a\right)\lambda + a^{-1} = 0. \tag{28}$$

This gives

$$\begin{aligned}\text{Real}\,(\lambda_{\text{phugoid}}) &= -\frac{\eta C_{D_0}}{\omega}\left(1+\left(\frac{\xi}{\omega}\right)^2 a\right)\\ \text{Im}\,(\lambda_{\text{phugoid}}) &= \left[1-\left(\frac{\eta C_{D_0}}{\omega}\right)^2\left(1+\left(\frac{\xi}{\omega}\right)^2 a\right)\left(1-3\left(\frac{\xi}{\omega}\right)^2 a\right)\right]^{1/2}\end{aligned} \tag{29}$$

With the roots calculated we have for the spiral mode in real time

$$t_{\text{double}} = \frac{0.69\text{ m}}{\varrho_0 S C_{D_0} u_0}\left(\frac{\omega}{\xi}\right)^2\left[1+\left(\frac{2\eta C_{D_0}}{\omega}\right)^2\left(\frac{\xi}{\omega}\right)^2 a\left(1+\left(\frac{\xi}{\omega}\right)^2 a\right)\right]. \tag{30}$$

For the phugoid mode the damping is given by

$$t_{\text{half}} = \frac{1.38\text{ m}}{\varrho_0 S C_{D_0} u_0} \times \frac{1}{1+\left(\frac{\xi}{\omega}\right)^2 a}. \tag{31}$$

In real time, the phugoid period is

$$P = \frac{2\pi u_0}{\omega g_0}\left[1-\left(\frac{\eta C_{D_0}}{\omega}\right)^2\left(1+\left(\frac{\xi}{\omega}\right)^2 a\right)\left(1-3\left(\frac{\xi}{\omega}\right)^2 a\right)\right]^{-1/2}. \tag{32}$$

In the last equation, by taking the bracket equal to unity we have a result that is identical to Laitone and Chou's Equation (1.5) (1965). At very high altitudes, ω tends to unity and ϱ tends to zero. The phugoid period asymptotically tends to the circular orbital period. In reality, after a perturbation has been applied in a vacuum, the vehicle will go into a slightly elliptical orbit. Thus, P should tend to this elliptic orbital period. This correct orbital period appears only when we consider non-linear terms.

In general, the quantity $(2\eta C_{D_0}/\omega)^2\,(\xi/\omega)^2$ in the expansion of a, Equation (27), is small and setting $a=1$ gives a very good approximation. This expansion gives the roots of the characteristic equation explicitly to the desired degree of accuracy. In our derivation, the damping term for the phugoid is

$$\exp\left[-\frac{\varrho_0 u_0 S C_{D_0}}{2m}\left(1+\left(\frac{\xi}{\omega}\right)^2 a\right)t\right] \tag{33}$$

where a is explicitly given by the series expansion, Equation (27). Using $a=1$ we have Laitone and Chou's Equation (3.9) for phugoid damping. Hence, besides the additional spiral mode obtained, the above results improve the already accurate formulas of Laitone and Chou (1965) through the use of the correctional factor a.

The quantities $(\xi/\omega)^2$, ω^2 and a are plotted in Figures 5 and 6 as functions of the altitude. The value of a differs from unity by a maximum of about 4.5% near 300000 ft altitude. This is the altitude where the density gradient σ_1 is also a maximum as shown in Figure 4.

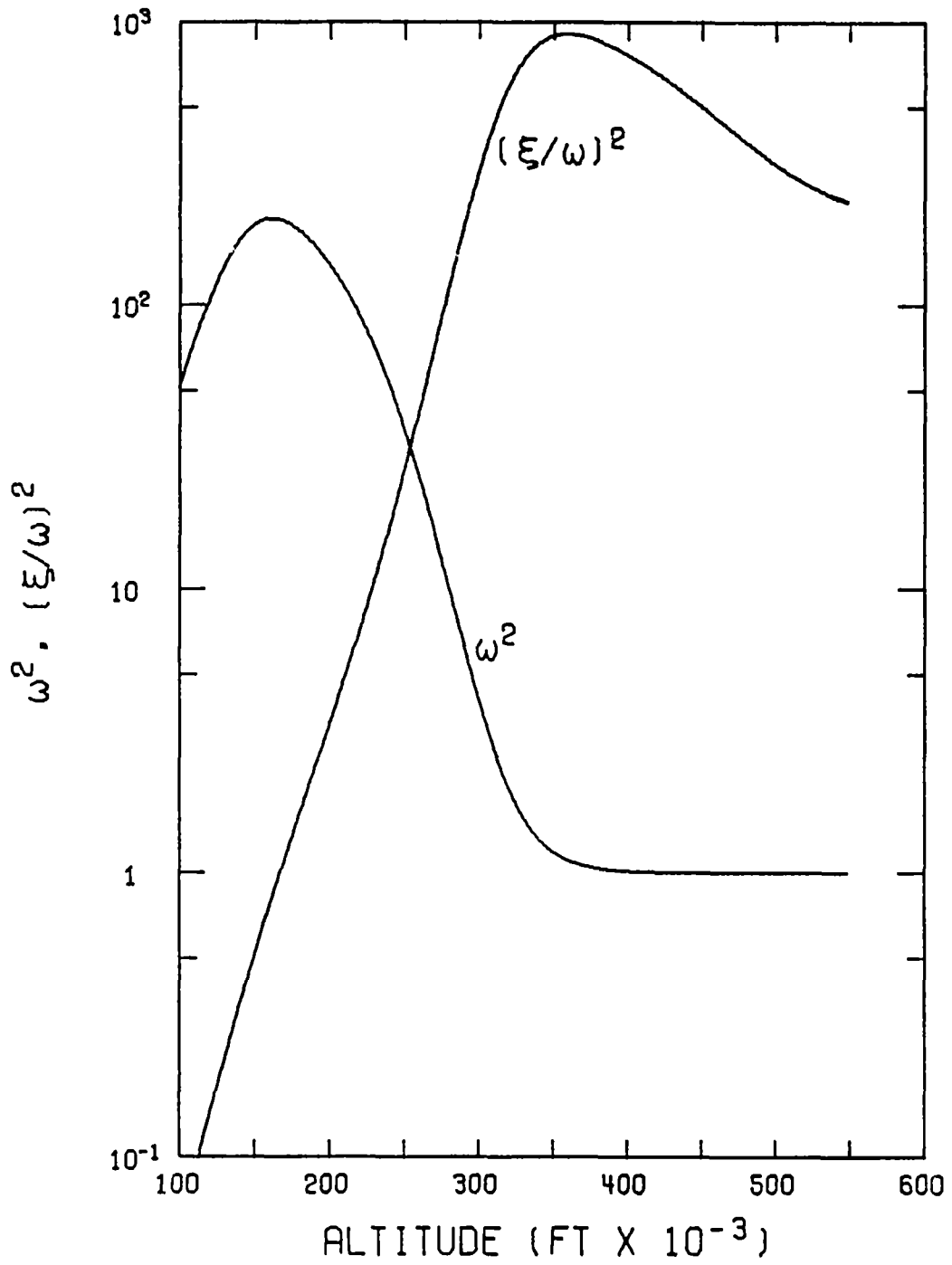

Fig. 5. Phugoid parameters, ω^2 and $(\xi/\omega)^2$.

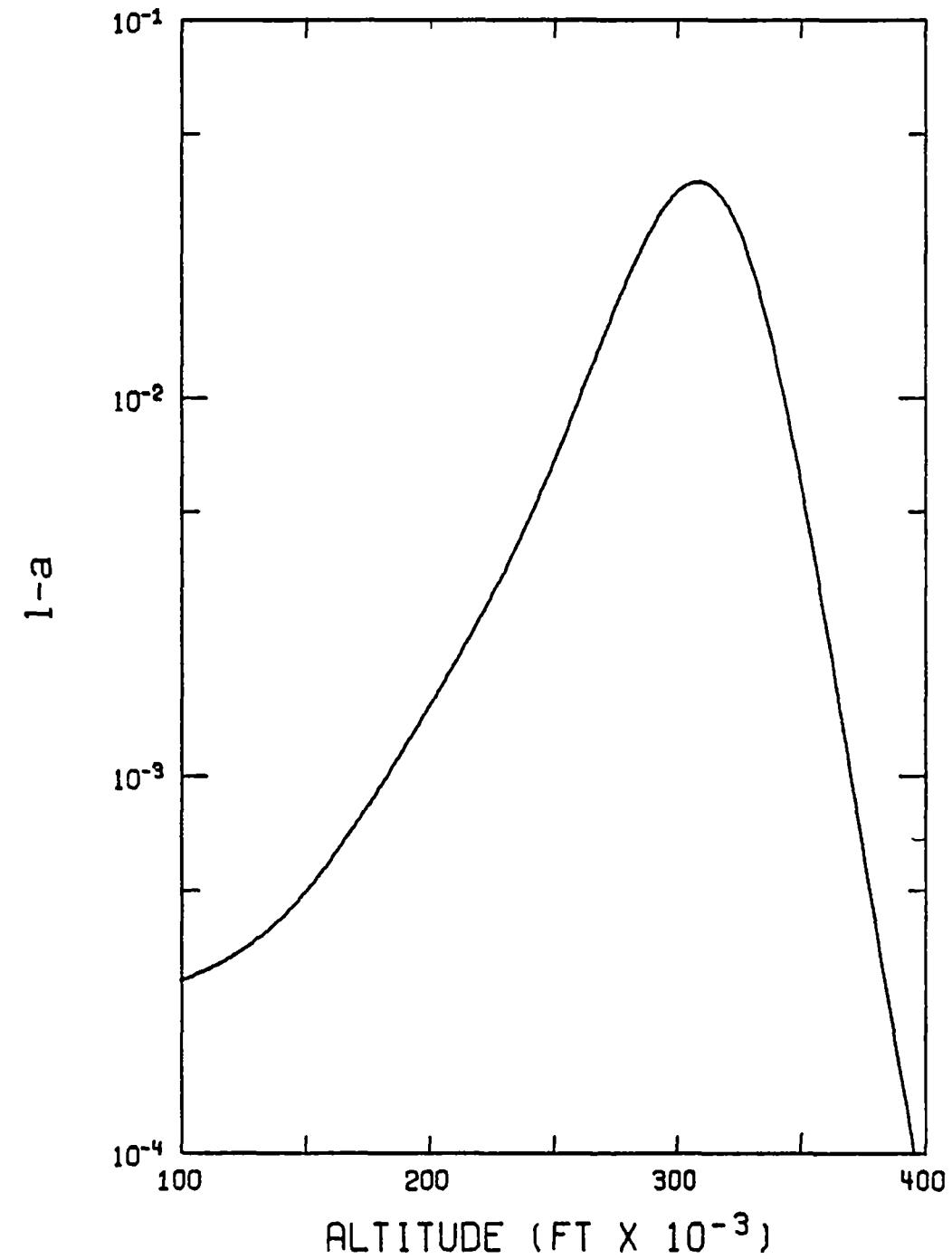

Fig. 6. Correction factor, *a*.

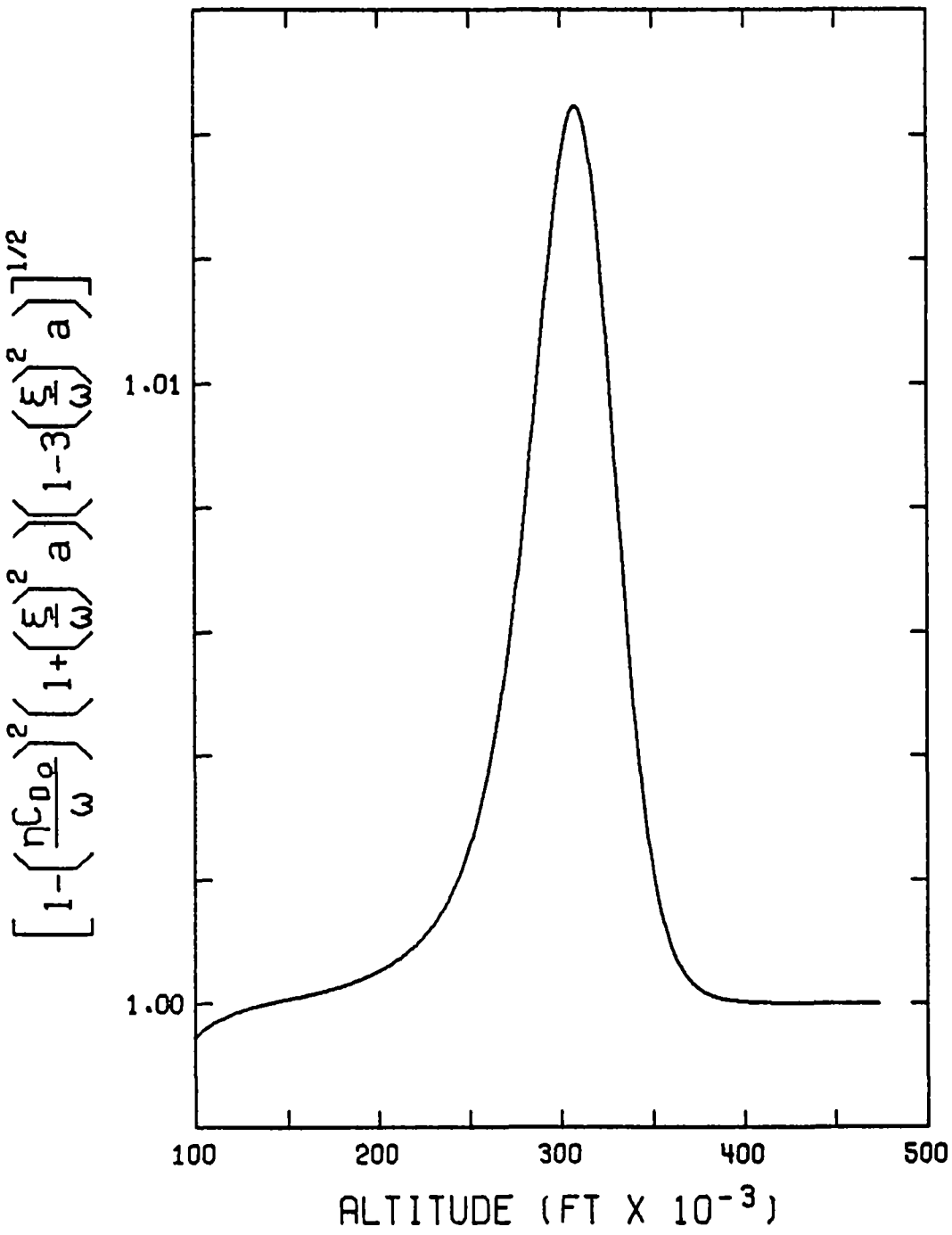

Fig. 7. Phugoid frequency correction factor.

In Equation (32), ω is the undamped natural frequency of the linear uncoupled phugoid motion. Hence the inverse of the bracket represents the drag correction factor to this natural frequency. The drag correction factor is plotted in Figure 7 and has a maximum contribution of about 1.4% at an altitude of 300000 ft.

Now let

$$\begin{aligned} \lambda_{\text{phugoid}} &= \lambda_1 \pm i\omega_1 \\ \lambda_{\text{spiral}} &= \lambda_2 . \end{aligned} \tag{34}$$

With the roots calculated, we have, to the first order, for the elements of the flight path

$$\begin{aligned} \hat{r} &= 1 + \varepsilon C_1 e^{\lambda_2 \tau} + \varepsilon e^{\lambda_1 \tau}[C_2 \cos \omega_1 \tau + C_3 \sin \omega_1 \tau] \\ \gamma &= \frac{\varepsilon \omega \lambda_2}{s^2} C_1 e^{\lambda_2 \tau} + \frac{\varepsilon \omega}{s^2} e^{\lambda_1 \tau}[(\omega_1 C_3 + \lambda_1 C_2) \cos \omega_1 \tau \\ &\quad - (\omega_1 C_2 - \lambda_1 C_3) \sin \omega_1 \tau] \\ \hat{u} &= 1 + \frac{\varepsilon}{2s^2}[(\omega^2 - 2) + \omega^2 \lambda_2^2] C_1 e^{\lambda_2 \tau} \\ &\quad + \frac{\varepsilon}{2s^2} e^{\lambda_1 \tau}\{[[(\omega^2 - 2) + \omega^2 (\lambda_1^2 - \omega_1^2)] C_2 + 2\omega^2 \omega_1 \lambda_1 C_3] \cos \omega_1 \tau \\ &\quad + [[(\omega^2 - 2) + \omega^2 (\lambda_1^2 - \omega_1^2)] C_3 - 2\omega^2 \omega_1 \lambda_1 C_2] \sin \omega_1 \tau\} \end{aligned} \tag{35}$$

where the C_i are constants of integration.

From these expressions we have the following interesting remarks:

(1) In each of the variations of elements such as radial distance, flight path angle, and velocity, there are two components. One component is oscillatory with diminishing amplitude and it tends to circularize the flight path. The other component is aperiodic and divergent. This component is due to the offset effect between the thrust and the drag and induces a secular variation of the elements of the orbit.

(2) For the example vehicle, $\omega_1 > 1$ above about 140000 ft and $\omega_1 \to 1$ as $r_0 \to \infty$, thus the effect of drag is to shorten the phugoid period.

(3) In the expression for $\hat{r}$, since $\lambda_2 > 0$, the divergent mode tends to decrease the radial distance if the initial perturbations are such that $\varepsilon C_1 < 0$. On the contrary if $\varepsilon C_1 > 0$ the radial distance will increase with time. Furthermore, under the constant thrust application, with decreasing drag the vehicle will move outward following a spiral.

(4) From the expression for the flight path angle we see that it varies in the same direction as the radial distance.

(5) On the contrary, the velocity varies as the radial distance if and only if

$$\omega^2 > \frac{2}{1 + \lambda_2^2}. \tag{36}$$

If the inequality is satisfied the velocity will increase as the vehicle is spiraling out and decrease if the vehicle is spiraling in. The inverse is true if the inequality reverses. To calculate the altitude where the velocity inversion occurs, since λ_2^2 is small, we can use the equation

$$\omega^2 = 2. \tag{37}$$

From Figure 5, we see that ω^2 is large at low altitudes and tends asymptotically to 1 when the altitude increases indefinitely. When $\omega^2 = 2$ the velocity inversion occurs. More explicitly, using the definitions in Equations (5) and (10) we have

$$\frac{(W/S)_s}{C_{L_0}} = -\frac{g_s r_0 \varrho_0}{2}(2 + \sigma_1) \tag{38}$$

where subscript, s, denotes the condition at sea level. The left-hand side of the formula above is a characteristic of the vehicle and the right-hand side is solely dependent on the characteristics of the atmosphere. Figure 8 is a plot of Equation (38) as a function of altitude and the graph can be used to determine the altitude where the velocity inversion occurs for any given vehicle. For the example vehicle, we have $(W/S)_s/C_{L_0} = 600$ lb/ft^2. Thus, the critical altitude for velocity inversion is 321000 ft.

(6) To the first order, the phugoid period tends to the circular orbital period when the altitude of flight increases indefinitely. In reality, the phugoid period tends to the perturbed elliptical period. To find this correct orbital behavior we use a new time variable, $\bar{t}$, such that

$$\bar{t} = \tau(1 + h_1\varepsilon + h_2\varepsilon^2 + \cdots)^{-1}$$

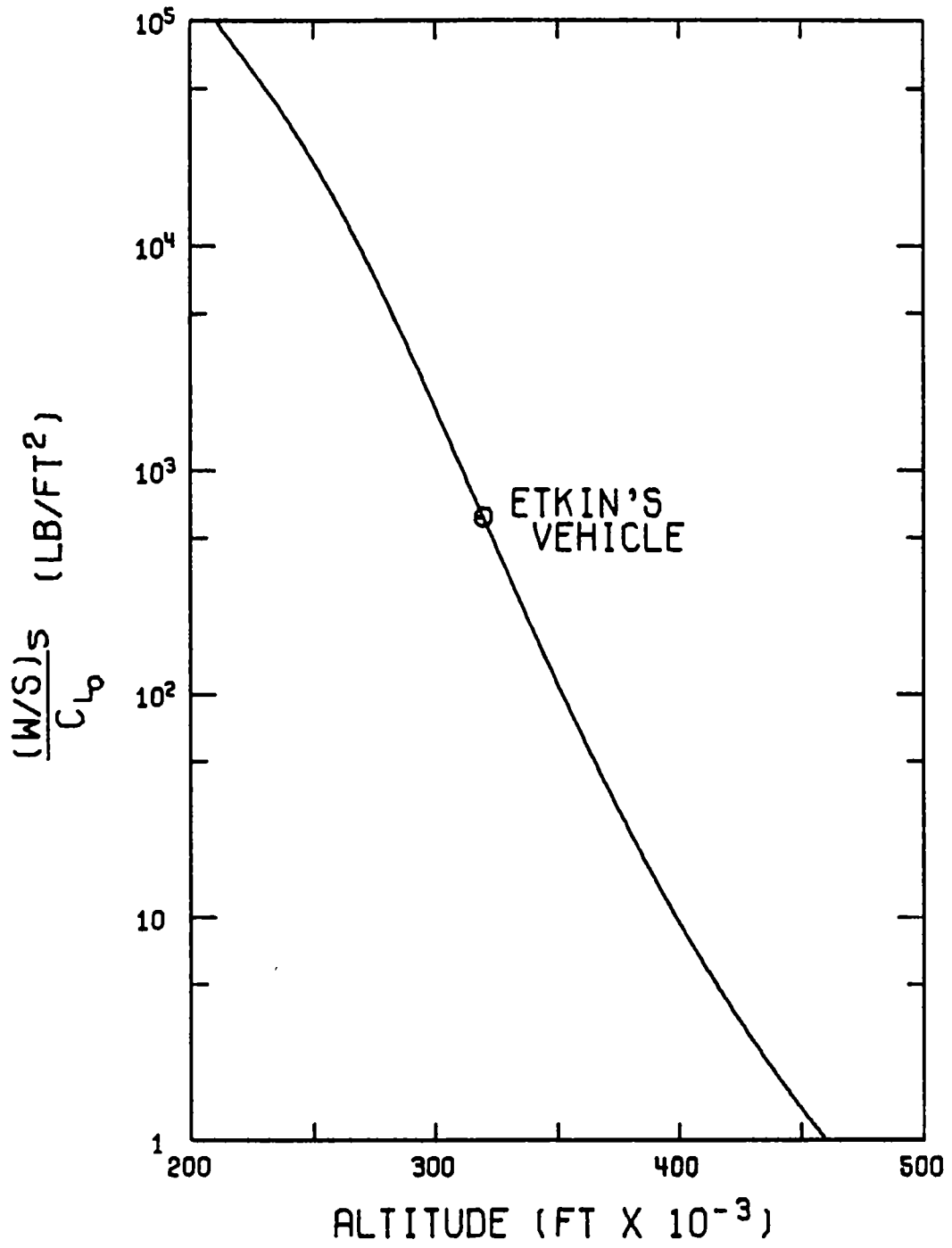

Fig. 8. Speed perturbation inversion altitude.

where h_1, h_2 are constants to be determined. By substituting into Equation (21), neglecting drag terms, and requiring a periodic solution for $\bar{X}$, we can easily find that

$$-h_1 = \frac{(\omega^2 - 2)^2 - 2(1 - s^2)(\omega^2 - 2) + 4s^2(\beta - 2)}{s^2\omega^4}. \tag{39}$$

Hence, to the first order, an asymptotic expression for the phugoid period is

$$P = \frac{2\pi u_0}{\omega g_0}(1 + \varepsilon h_1 + \cdots). \tag{40}$$

The time constants and the period of the spiral and phugoid mode motions, obtained numerically from the fifth-order characteristic equation of the coupled linear system (First Equation (15)) are plotted as the solid curves in Figures 9–11. The values of these parameters predicted by Equations (30–32) are also plotted in the figures. The analytical solutions appear as dashed-line curves where they differ enough from the numerical solutions to resolve them. For reference, the time to complete one revolution of the Earth along the reference flight path is also plotted in the figures.

The two solutions for the spiral mode time constant (Figure 9) are in agreement to at least four significant figures in the altitude range 100–510000 ft. Near an altitude of 250000 ft the spiral mode gives important contributions to the vehicle motion, while above 400000 ft the effects are negligible.

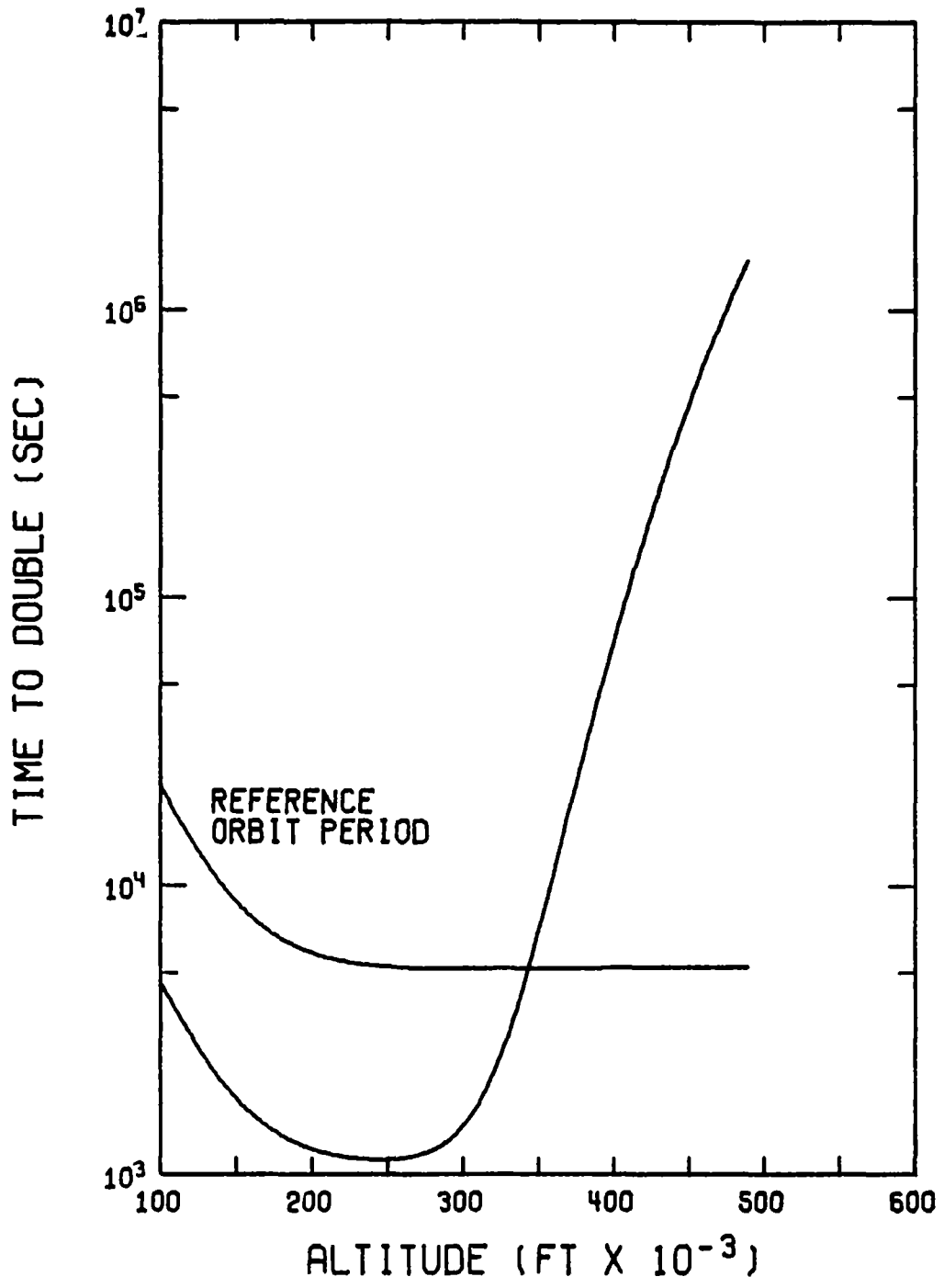

Fig. 9. Spiral mode time constant.

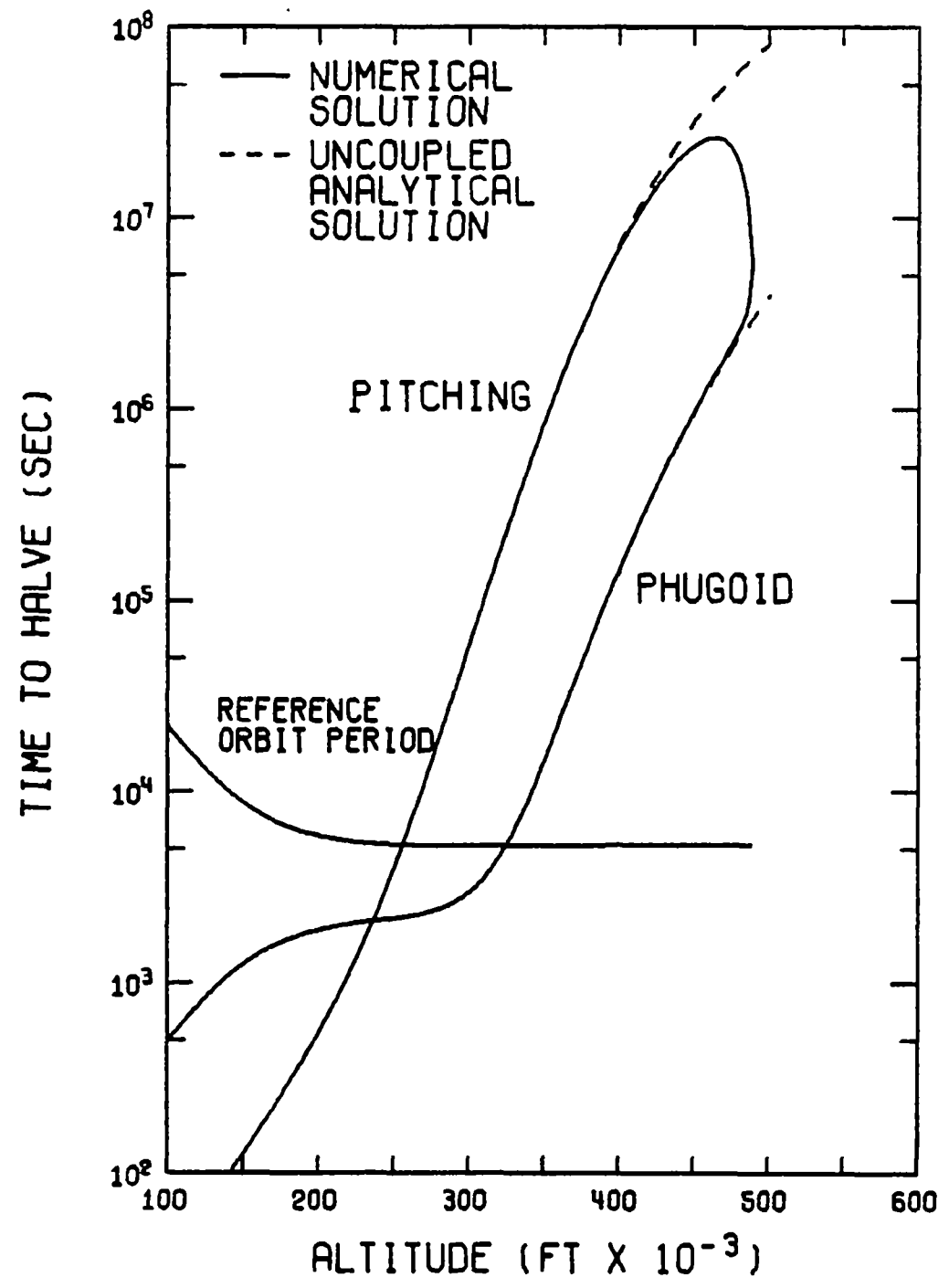

Fig. 10. Oscillatory mode time constants.

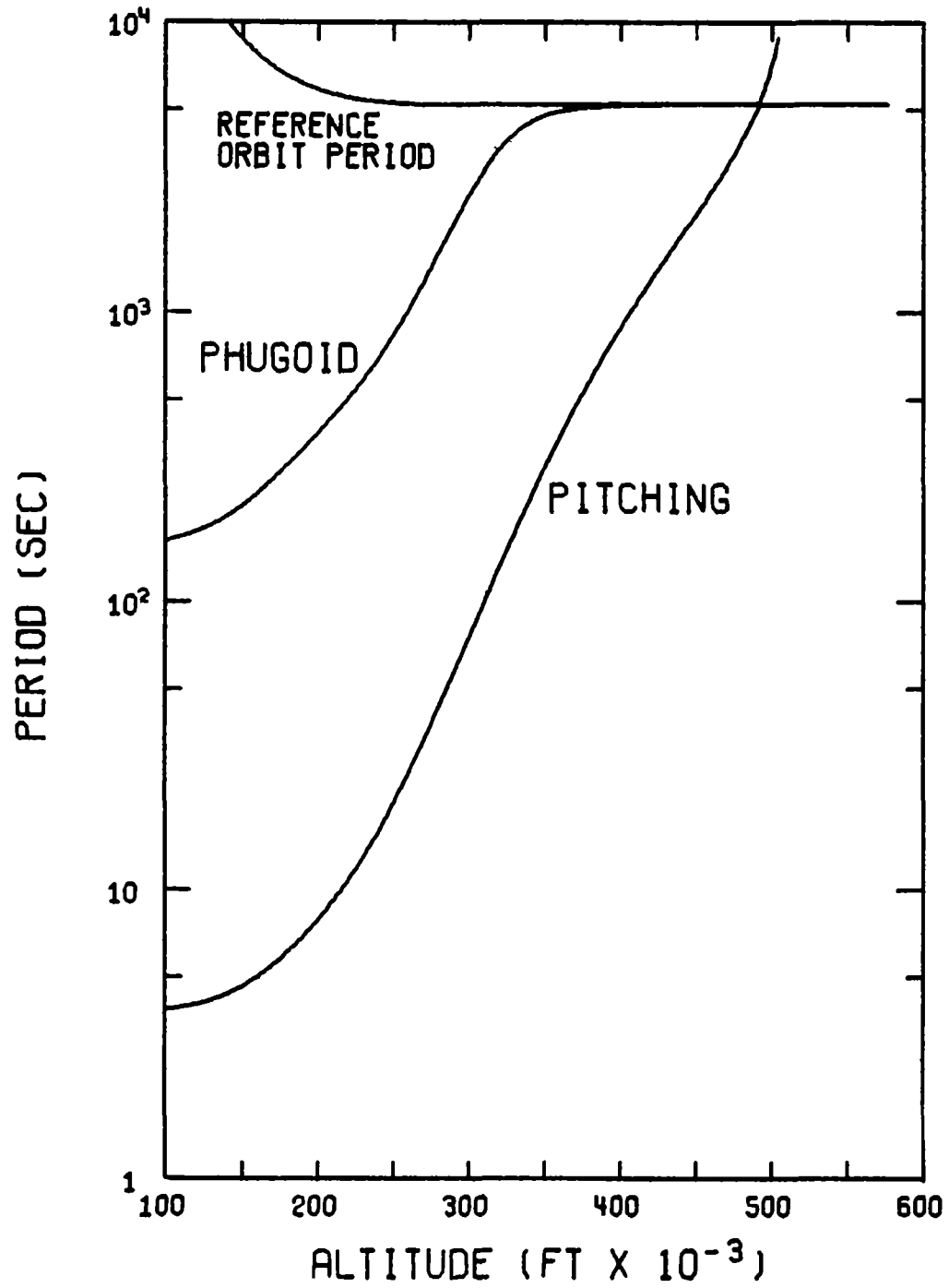

Fig. 11. Oscillatory mode periods.

The analytic solution for the phugoid time constant (Figure 10) is less accurate, agreeing with the numerical solution to only three significant figures in the altitude range of 100–450000 ft. Above 450000 ft altitude the two solutions diverge significantly and coupling effects must be considered to correctly predict the perturbed vehicle motion.

The two solutions for the phugoid period (Figure 11) agree to at least five significant figures in the altitude range of 100–490000 ft.

B. PITCHING MODE

The equations of motion governing the pitching mode motion are given by the last two components of Equations (15). Since the uncoupled spiral and phugoid mode motions have been determined, we can write these equations as a matrix differential equation with a forcing function. Thus

$$\hat{X}_1' = A_2 \hat{X}_1 + C(\bar{X}_1) \tag{41}$$

where

$$\hat{X}_1 = \begin{bmatrix} \hat{q}_{11} \\ \alpha_{11} \end{bmatrix} \qquad A_2 = \frac{1}{\omega} \begin{bmatrix} -\eta(C_{N_1} - C_{N_2}) & -\dfrac{n^2}{s^2} \\ s^2 & -\eta(C_{N_1} + C_{N_2}) \end{bmatrix}$$

$$C(\bar{X}_1) = \frac{1}{\omega} \begin{bmatrix} -3k_0\gamma_{11} \\ -(2 - s^2)\,\hat{u}_{11} + \dfrac{\omega^2 - (2 + s^4)}{s^2}\,\hat{r}_{11} \end{bmatrix}. \tag{42}$$

The matrix C can be expressed as a function of the non-dimensional time τ by substituting the appropriate linear phugoid solution. Then, by integrating Equation (41) we have

$$\hat{X}_1 = e^{A_2\tau}\hat{X}_1^0 + \int_0^\tau e^{A_2(\tau-t)}C(t)\,dt \tag{43}$$

where

$$\hat{X}_1^0 = \hat{X}_1(0). \tag{44}$$

The unforced system has the characteristic equation

$$\lambda^2 + \frac{2\eta C_{N_1}}{\omega}\lambda + \left(\frac{n}{\omega}\right)^2\left[1 + \left(\frac{\eta}{n}\right)^2(C_{N_1}^2 - C_{N_2}^2)\right] = 0 \tag{45}$$

which, in turn, has the complex conjugate roots

$$\lambda_{\text{pitch}} = -\frac{\eta C_{N_1}}{\omega} \pm i\frac{n}{\omega}\left[1 - \left(\frac{\eta C_{N_2}}{n}\right)^2\right]^{1/2}. \tag{46}$$

With these roots it is now possible to determine the exponential matrix $e^{A_2\tau}$ and hence to solve for the pitching mode motion from Equation (43). We first restrict the discussion to an investigation of the pitching mode characteristic roots, Equation (46).

For the example vehicle, the quantity n^2 (see Equations (10)) is positive below and negative above an altitude of about 513000 ft. The constant C_{N_1} is positive. Hence, for perturbations in a pitching variable, the vehicle will oscillate with diminishing amplitude about the vehicle's center of mass below an altitude of 513000 ft. Above this altitude the gravity torque is larger than the aerodynamic torque and the pitching mode diverges. Thus, the altitude where $n^2 = 0$ represents a limit below which the vehicle attitude is aerodynamically stabilized.

The pitching mode oscillations will diminish to half amplitude in the time

$$t_{\text{half}} = \frac{1.38\text{ m}}{\varrho_0 S u_0 C_{N_1}} \tag{47}$$

and have a period of

$$P = \frac{2\pi u_0}{g_0 n}. \tag{48}$$

The quantity $(\eta C_{N_2}/n)^2$ has been omitted from Equation (48) because it's effect is negligible at all altitudes.

Equations (47) and (48) are compared graphically, as was done with the spiral and phugoid modes, with the time constant and period obtained numerically from the fifth-order characteristic equation in Figures 10 and 11. Again, the solid curves represent the numerical solutions and the dashed-line curves represent the analytical solutions where they differ enough from the numerical solutions to resolve them. The two values for the time constant (Figure 10) are in agreement to 3 significant

figures in the altitude range of 100–350000 ft. Above 350000 ft the two solutions diverge and, as was the case with the phugoid time constant, coupling effects must be considered. We see that the pitching mode is heavily damped in the lower altitude range while it is negligibly damped in the higher altitude range. Again, as was the case with the phugoid mode, the two solutions for the pitching mode period (Figure 11) are in agreement to 5 significant figures in the altitude range of 100–490000 ft.

The expression for the pitching mode damping constant $-(\eta C_{N_1}/\omega)$ is the same, except for notational differences, as Laitone and Chou (1965) Equation (4.8), but our expression for the frequency (n/ω), which contains the ratio k_0, is valid for more general body shapes.

C. RESONANCE ALTITUDE

In Figure 11 we see that, as the altitude increases, the uncoupled pitching mode period approaches that of the phugoid mode and exceeds it, slightly above 490000 ft. When the two periods are equal, since the forcing term in Equation (41) has the same frequency as the natural pitching frequency, resonant oscillations will build up if the uncontrolled vehicle remains at the same altitude. The altitude where the two periods are equal, called the resonance altitude, is found by solving the equation $\omega = n$.

Substituting the definitions from Equation (10) and, for simplicity, setting $s^2 = 1$, we separate the equation into vehicle and atmospheric characteristics as was done for

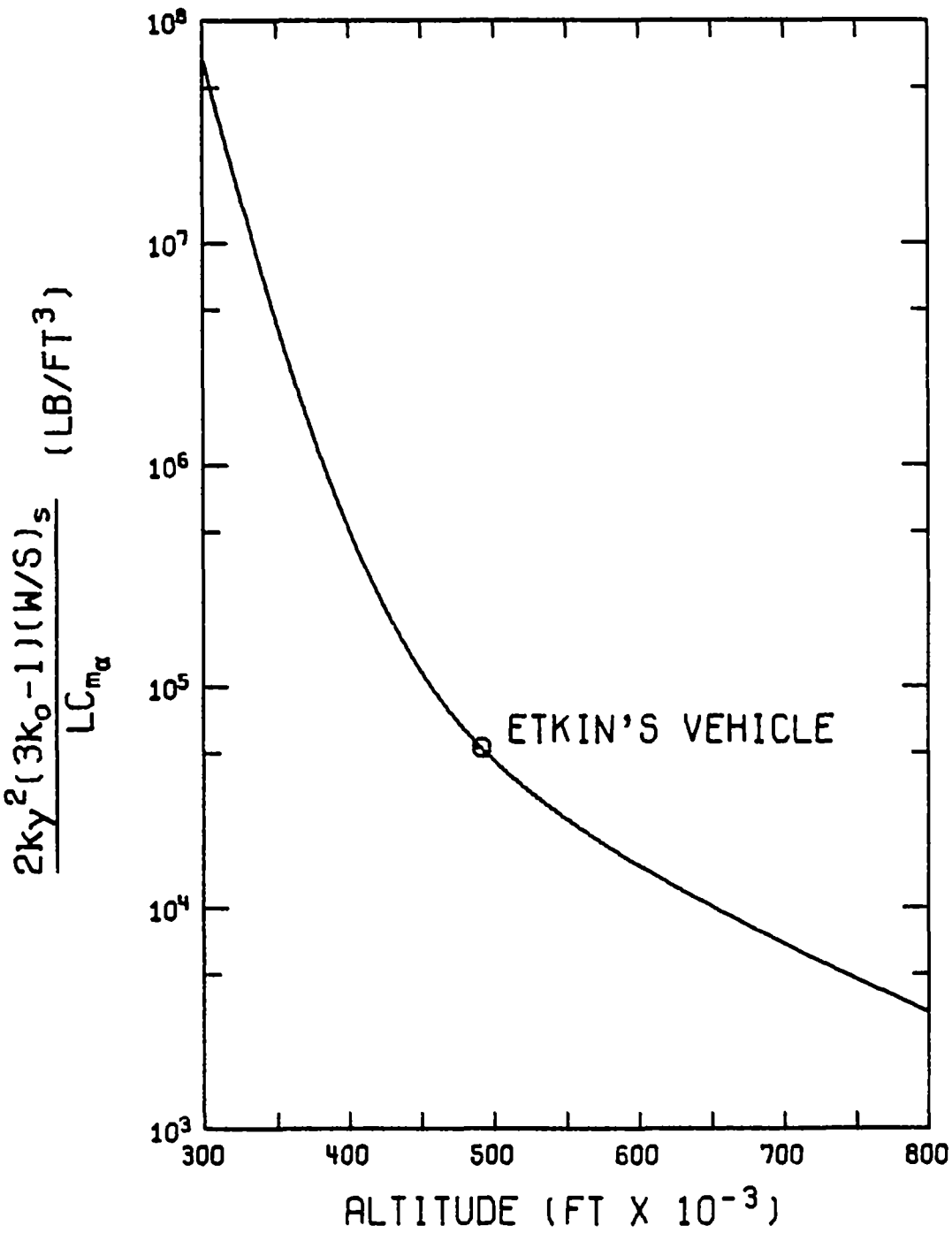

Fig. 12. Resonance altitude.

the speed perturbation inversion altitude. Thus, we have

$$\frac{2k_y^2(3k_0 - 1)(W/S)_s}{LC_{m_\alpha}} = \varrho_0 r_0^2 g_s \tag{49}$$

where subscript s again denotes sea level conditions. Plotting the right hand side of this equation as a function of altitude we can find the resonance altitude for any given vehicle configuration. From Figure 12 we find that for the example vehicle the altitude is 492 300 ft.

D. COUPLING EFFECTS

The linear analytical solutions for the uncoupled oscillatory mode characteristics, Equations (29) and (46), show that the damping constants remain negative at all

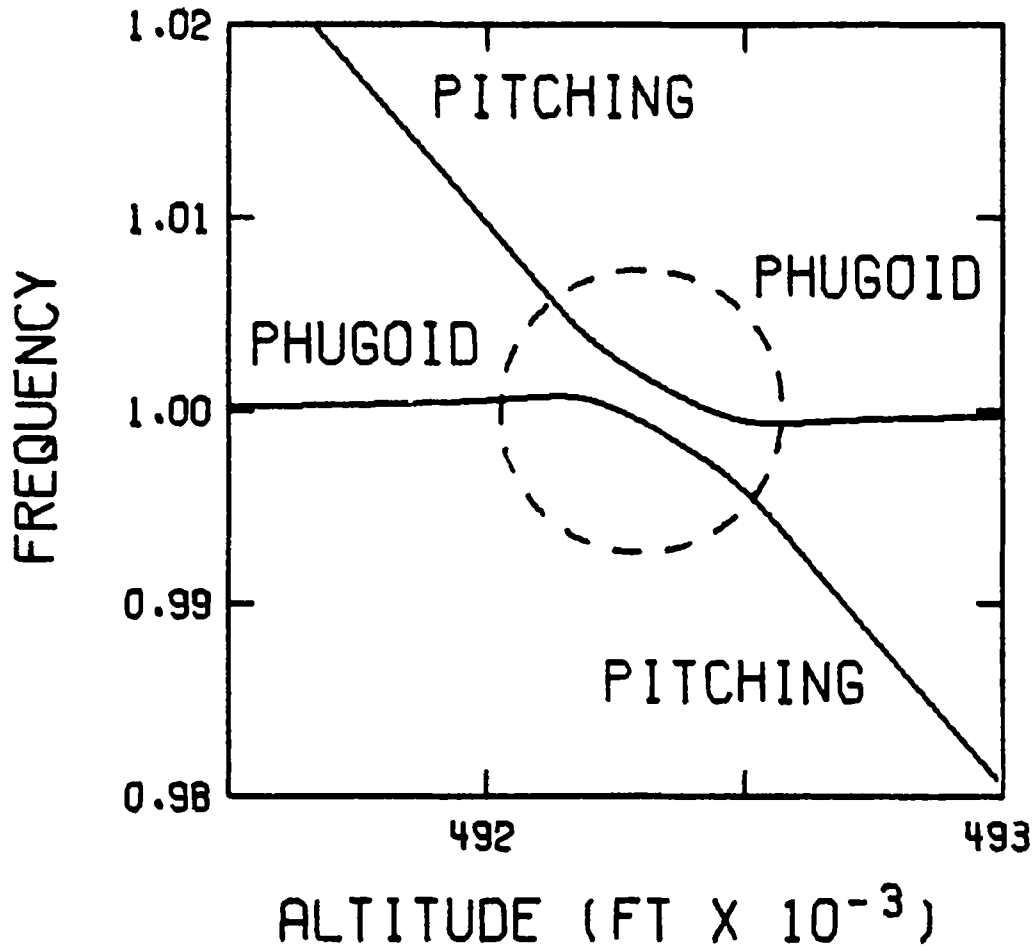

Fig. 13. Frequencies near resonance altitude.

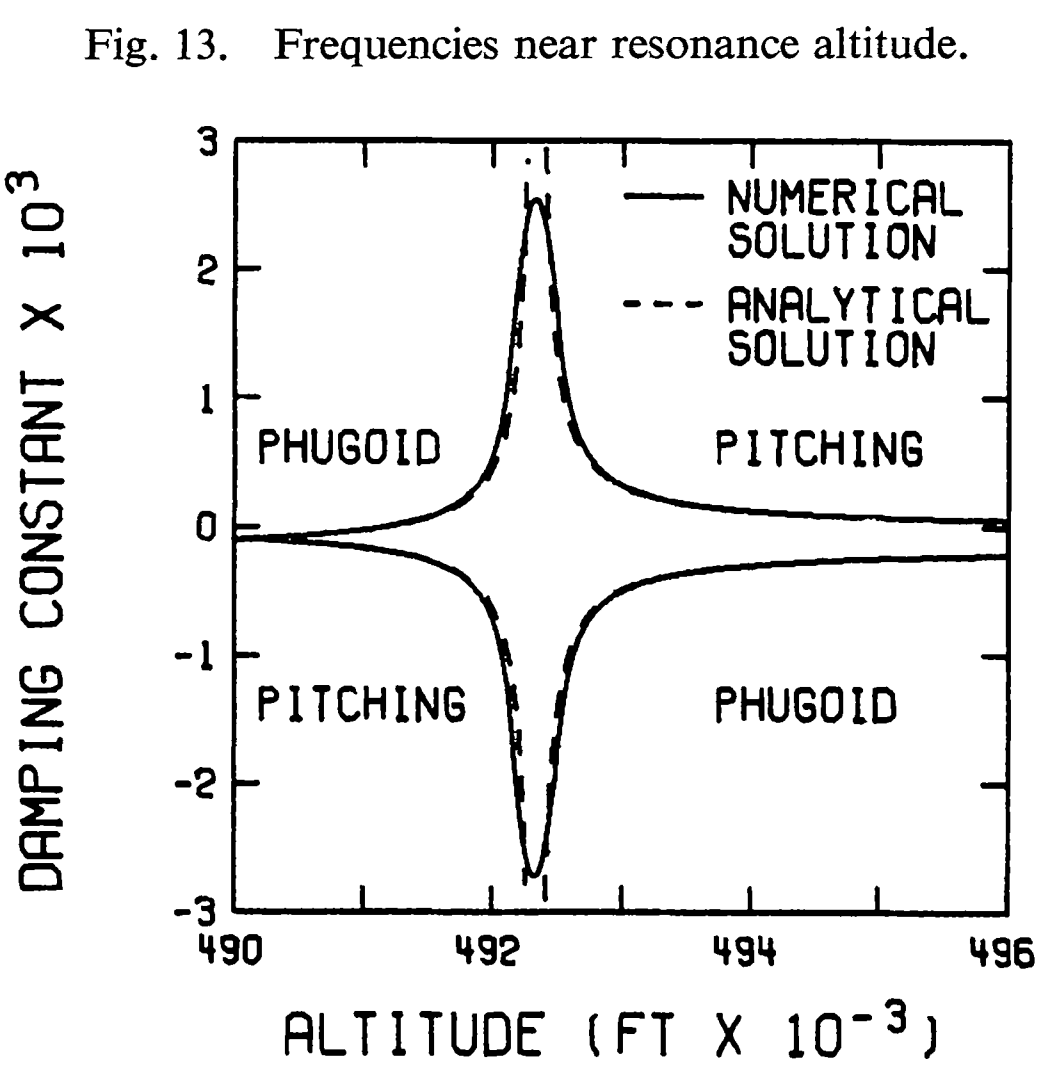

Fig. 14. Damping constants near Resonance altitude.

altitudes and that the frequencies 'cross-over' each other at the resonance altitude. However, a close examination of the numerical solutions of the fifth-order coupled characteristic equation near the resonance altitude reveals these behaviors to be in error and reveals, instead, the phenomena shown in Figures 13 and 14.

We see that instead of a 'crossing' of the mode frequencies, there is, in fact, a 'switching' of the mode frequencies at the resonance altitude. The modes must 'switch' since we have shown previously that the phugoid mode frequency must tend asymptotically to the reference orbit frequency as the atmospheric density tends to zero.

In Figure 14 we see that near the resonance altitude the phugoid mode damping constant becomes positive and the mode becomes unstable, while the pitching mode damping constant remains negative. Above the resonance altitude the 'switched' pitching mode damping constant is positive while that of the 'switched' phugoid is negative. Since the pitching mode damping constant is unstable above the resonance altitude, this altitude is the limit below which the vehicle's attitude can be aerodynamically stabilized and not the altitude where $n^2 = 0$ predicted by the uncoupled mode characteristics.

The fifth-order coupled characteristic equation

$$|\lambda I - A| = 0 \tag{50}$$

where I is the unit matrix and A is defined by Equation (12), can be factored empirically to take into account some of the effects described above. By performing simple column and row operations on Equation (50) we factorize the equation into the form

$$(\lambda^3 + a_1\lambda^2 + a_2\lambda + a_3)(\lambda^2 + b_1\lambda + b_2) + (c_1\lambda + c_2) = 0 \tag{51}$$

where

$$a_1 = \frac{2\eta C_{D_0}}{\omega} - K\frac{\eta}{2\omega}(C_{N_1} + C_{N_2})$$

$$a_2 = 1 + 0(\eta^2)$$

$$a_3 = -\frac{2C_{D_0}}{\omega}\left(\frac{\xi}{\omega}\right)^2 + 0(\eta^2)$$

$$b_1 = \frac{2\eta C_{N_1}}{\omega} + K\frac{\eta}{2\omega}(C_{N_1} + C_{N_2}) \tag{52}$$

$$b_2 = \left(\frac{n}{\omega}\right)^2 + 0(\eta^2)$$

$$c_1 = 0(\eta^2)$$

$$c_2 = 0(\eta^2)$$

$$K = \frac{2[s^2(1+s^2) + 3k_0 s^2 - \omega^2]}{\omega^2[1 - (n/\omega)^2]}$$

and the quantity $0(\eta^2)$ consists of terms of order of magnitude η^2 and smaller.

Neglecting the quantities $0(\eta^2)$ and factorizing the cubic and quadratic factors in Equation (51), as was done in the previous sections, we find that the spiral mode and the imaginary parts of the oscillatory mode roots are approximately unchanged while the damping constants take the forms

$$\text{Real}(\lambda_{\text{phugoid}}) = -\left[\frac{\eta C_{D_0}}{\omega}\left(1 + \left(\frac{\xi}{\omega}\right)^2 a\right) - K\frac{\eta}{4\omega}(C_{N_1} + C_{N_2})\right] \tag{53}$$

$$\text{Real}(\lambda_{\text{pitch}}) = -\left[\frac{\eta C_{N_1}}{\omega} + K\frac{\eta}{4\omega}(C_{N_1} + C_{N_2})\right] \tag{54}$$

where the quantity a is given by the series expansion (27).

With the coupling effect taken into consideration, the time constants derived from Equations (53) and (54) are now in agreement with the numerically derived time constants to about 5 significant figures in the altitude range of 100–490000 ft, and are indistinguishable from the values along the solid curves in Figure 10. Near the resonance altitude, Equations (53) and (54) are plotted in Figure 14 and appear as the dashed-line curves where they are resolvable from the numerical solutions. Thus, to within a few hundred feet below and above the resonance altitude, the uncoupled mode frequencies, ω and n, the coupled damping constants, Equations (53) and (54), and the spiral mode root, Equation (25), correctly and accurately predict the behavior of the linearized equations of motion, the first of Equations (15), at all altitudes above 100000 ft.

It must be emphasized, however, that since the spiral motion will take the vehicle through the exact resonance altitude, we would expect that perturbations in the phugoid variables would not lead to a pure resonance oscillation in the pitching mode variables, but would lead, instead, to the classical 'beating' phenomena, where the amplitudes of oscillation remain finite. A detailed examination of the pitching motion near the resonance altitude will be given in Chapter 4.

E. NONLINEAR SOLUTION

In the preceding sections we have only retained the linear term in the general solution, Equation (20). Uncoupled and coupled linear analytical solutions have been given and it has been shown that they are in excellent agreement with the numerically computed linear solution, namely Etkin's solution (Etkin, 1961). The next question to be answered is: how accurate is the linear solution, compared with the exact nonlinear solution?

The next higher order component of the vector state is $\varepsilon^2 X_2$. If $B(t) \equiv B(X_1)$, then

$$X_2 = \int_0^\tau e^{A(\tau - t)} B(t)\, dt \tag{55}$$

and, A and B are given by Equation (12) and X_1 represents the linear solution found in the preceding sections. Hence the computation of $X_2(\tau)$ is straightforward. Here

we need only to have an idea of the order of magnitude of the second order term. By the form of the vector $B(X_1)$, we can see that if the perturbation is small, the contribution of $\varepsilon^2 X_2$ is negligible. This has been shown in a numerical study by Rangi (1960). But in the expansion, Equation (8), of the mass density of the atmosphere, σ_2 is of the order 10^5 (see Figure 4). Hence, if $\varepsilon > 0(10^{-4})$ we should include the second order gradient effect of the air mass density, σ_2 which appears explicitly in $B(X_1)$. For the phugoid motion, Equation (21), terms which need to be retained in the phugoid component of the vector B are

$$B_1(\bar{X}_1) = \begin{bmatrix} -\dfrac{\eta C_{D_0}}{\omega}\sigma_2 \hat{r}_{11}^2 \\ -\dfrac{2\beta}{s^2\omega}\hat{r}_{11}^2 \\ 0 \end{bmatrix}. \tag{56}$$

Hence, the nonlinear numerical analysis of Rangi (1960) is not valid for large perturbations, since the author has neglected all second and higher order terms of the air mass density. For large perturbations, as were considered by Rangi (1960), the prime contributing nonlinear factor in the phugoid and spiral trajectory is the variation of the mass density of the atmosphere. The perturbed trajectories for these cases are highly eccentric orbits and it is not correct to assume a linear variation for the air mass density.

The value of σ_2 considered above is somewhat too large because of an inverse polynomial representation of the atmospheric mass density. This resulted from a curve fitting analysis which can give a wrong value for a truncated series at a certain altitude. In trajectory analysis a better approximation is usually found using an exponential atmosphere or, when an analytical solution of the trajectory is sought over a long interval of time, a simplified inverse polynomial atmosphere can be used. However, these model atmospheres are not suitable for a dynamic stability analysis in which a series expansion of the air mass density is required. In this paper we just want to call attention to the effect of the second and higher order atmospheric gradients. For an accurate second order analysis the coefficients σ_1 and σ_2 in the 'parabolic representation' of $\hat{\varrho}$, Equation (8), should be averaged for each limited altitude range considered. The effect of atmospheric mass density gradients can be dramatically illustrated by a numerical analysis.

Figures 15 and 16 respectively represent the variations of radial distance and flight path angle as time varies. They are reproductions of computer generated plots with different atmospheric mass density laws. The set is generated at an altitude of 300000 ft where the density gradients are the largest and with an initial nondimensional speed decrease of 10^{-3} ($\varepsilon = \Delta\hat{u} = -10^{-3}$). This corresponds to a perturbation of about 25 ft/sec.

The uncoupled, exact, nonlinear trajectory equations, the equations in $\hat{u}$, γ and $\hat{r}$ from Equations (6) with $\alpha = 0$, were integrated numerically, using the exact density

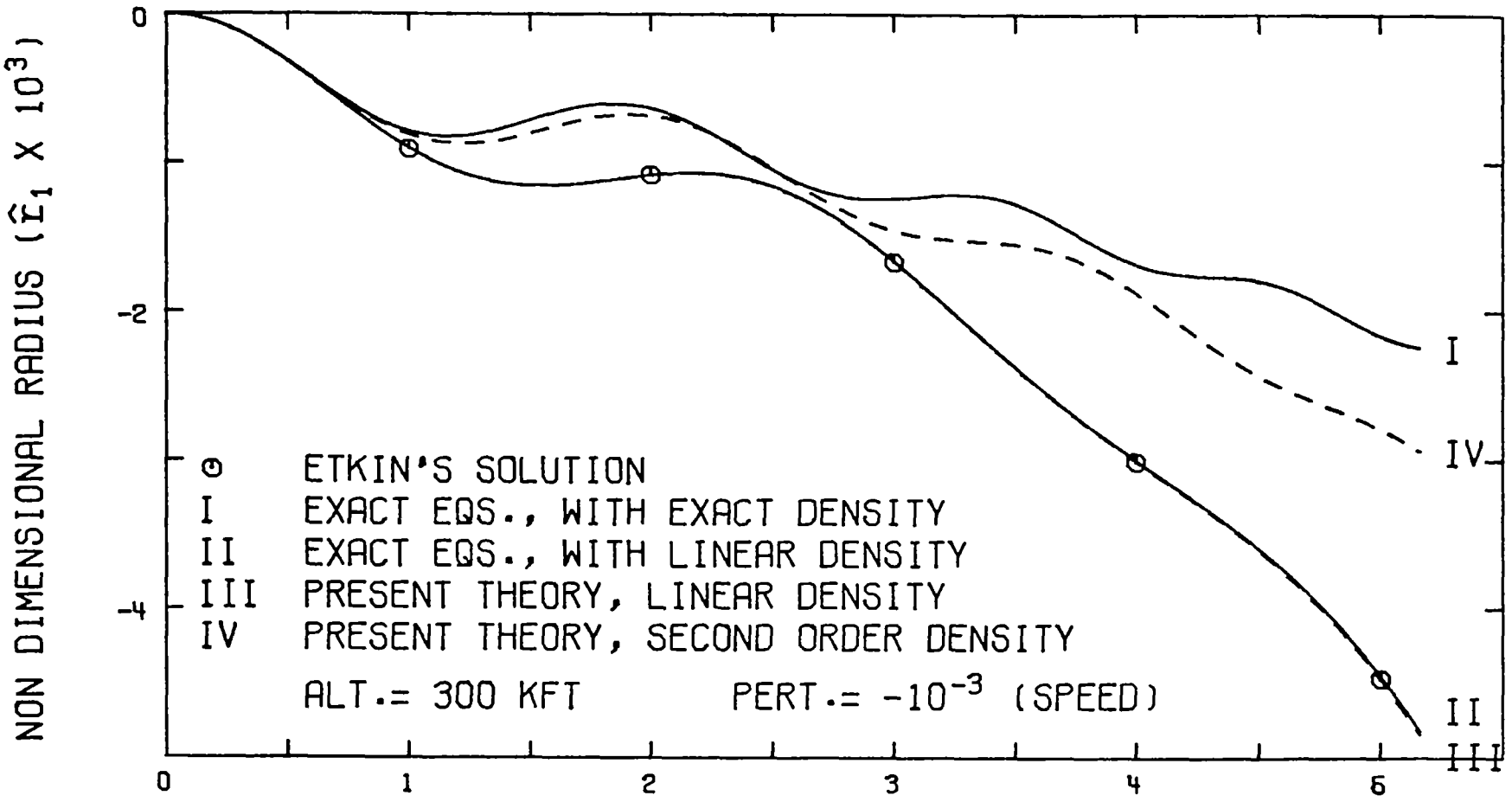

Fig. 15. Variation of radial distance.

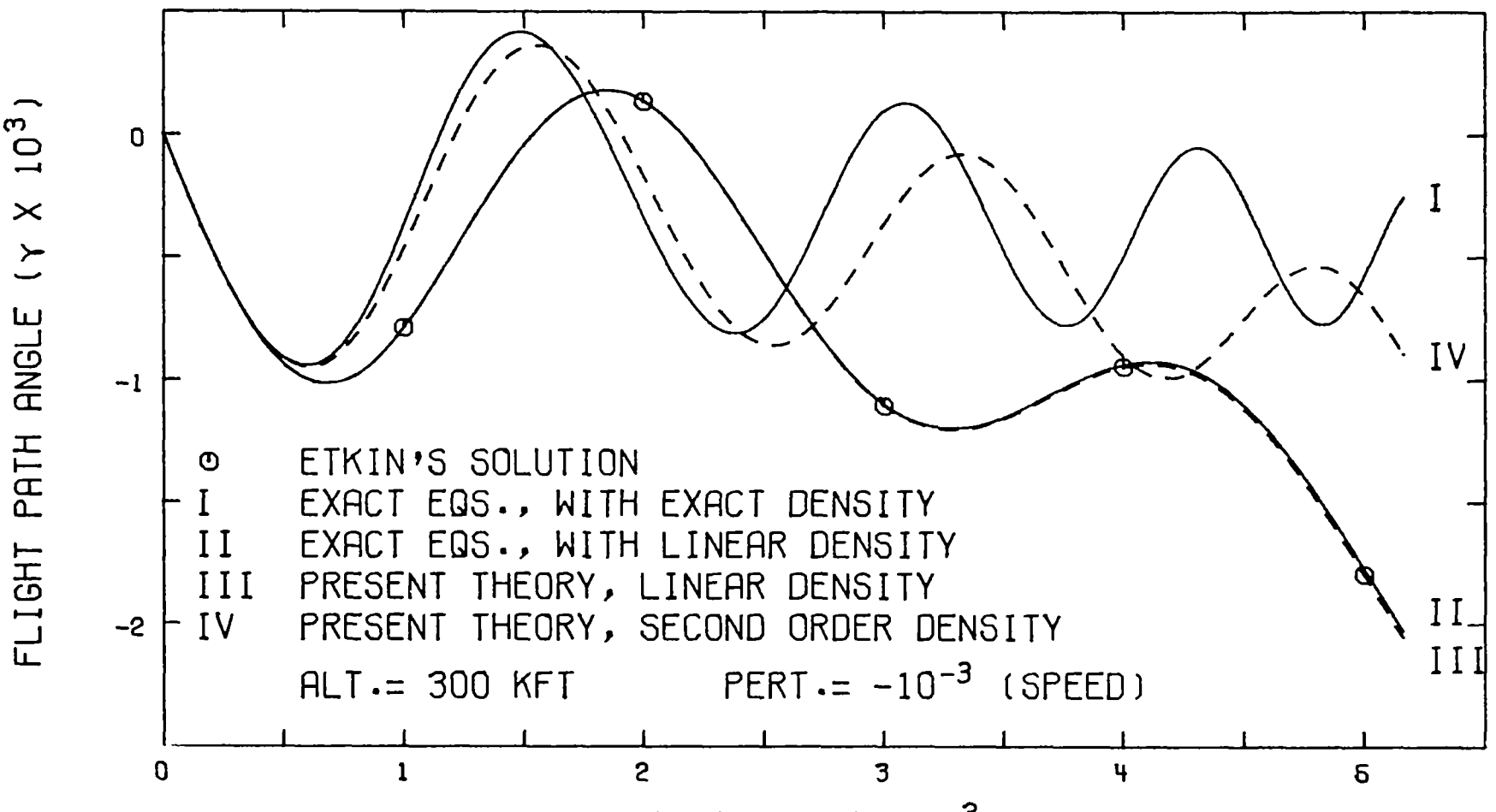

Fig. 16. Variation of flight path angle.

law, that is the 44th degree inverse polynomial representation of the *62 Standard Atmosphere*. The solutions are plotted in solid lines in Figures 15 and 16 as the curves I. A second set of curves, the curves II, were obtained by numerical integration of the nonlinear equations, but this time using a linear law for the mass density. The dotted lines, the curves III, represent the linear analytical solutions of the uncoupled motion in the present study with terms up to the order η^8 included in the value for a. For comparison the numerical solutions using Etkin's linearized coupled equations, Etkin, (1961) are also plotted. It is clear from the plots that our uncoupled, linear analytical

solutions and Etkin's linear coupled numerical solutions are nearly identical with the uncoupled exact solution with linear density. However, they do not compare well after $\frac{1}{4}$ of a revolution with the exact solution using the exact atmospheric mass density law. The former results can be improved by including higher order density gradients. The improvement is obtained by using the second order solution, Equation (21). These results are plotted in dotted lines as the curve IV. The discrepancies are much less at higher altitudes where atmospheric drag is small and at lower altitudes where the period is short and practical perturbations are small. The time scale taken for the plots is about 2 linear periods.

Referring to Figure 16 the flight path angle time history shows that the exact integration curve displays less spiral mode and less damping than the linear solution and further shows that the exact phugoid oscillations have smaller period. In fact the first cycle takes 1.95×10^3 sec versus the linear phugoid period of 2.51×10^3 sec. The second and third cycles take even less time and show that the exact motion will complete 3 cycles for the two linear periods.

A complete numerical analysis shows that below 100000 ft or above 400000 ft linear solutions are accurate. In between there is a definite requirement for the inclusion of higher order atmospheric mass density gradients.

4. Motion Near Resonance

The analysis in Chapter 3 shows that special care must be taken for the integration of the equations of motion near the resonance altitude. Fortunately, for a typical lifting vehicle as the one considered in this study, the resonance occurs at a high altitude where the drag is very small, and as far as the trajectory of the vehicle is concerned, it is practically a Keplerian orbit. On the contrary, near the resonance

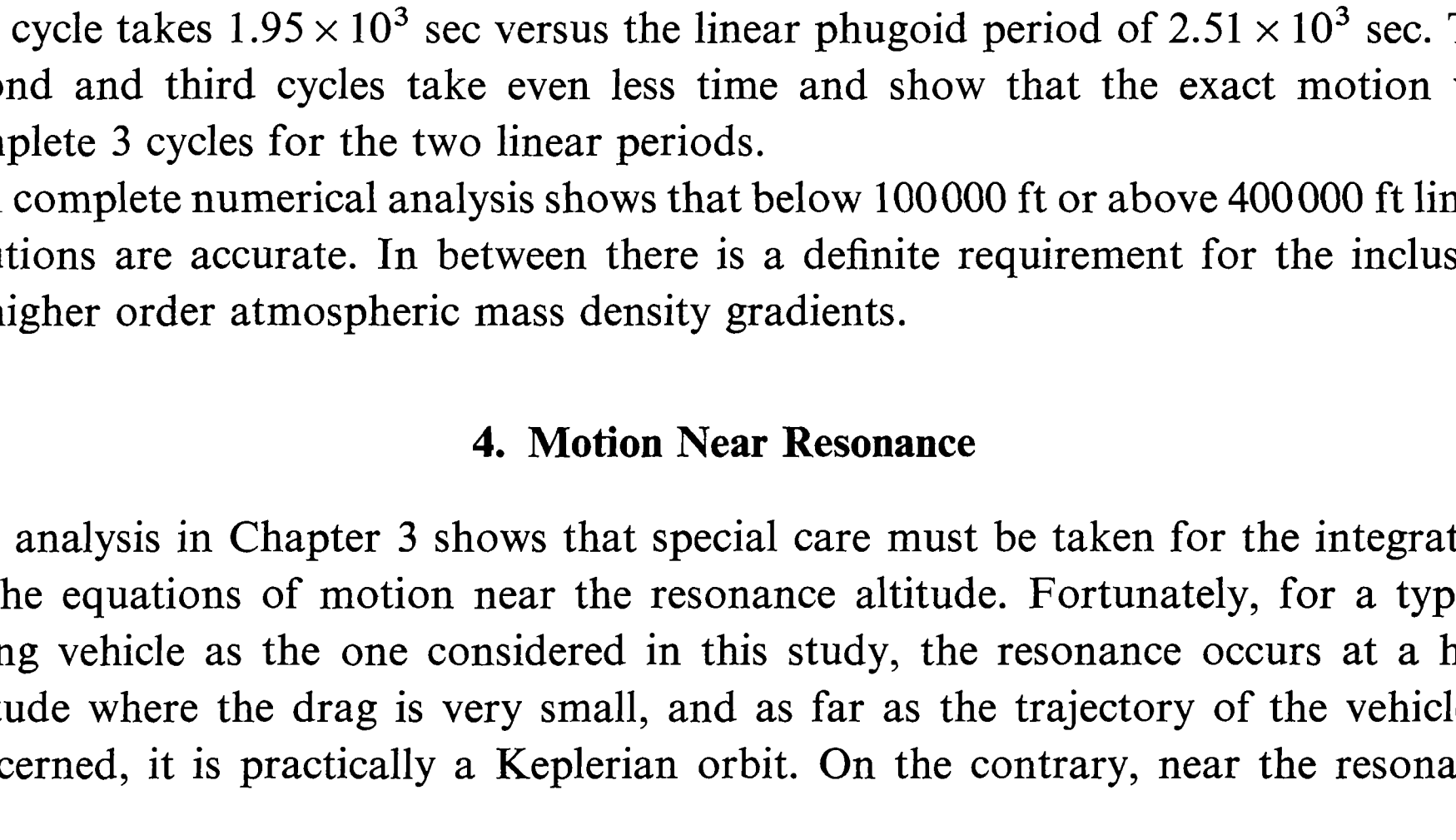

Fig. 17. Radial distance vs time.

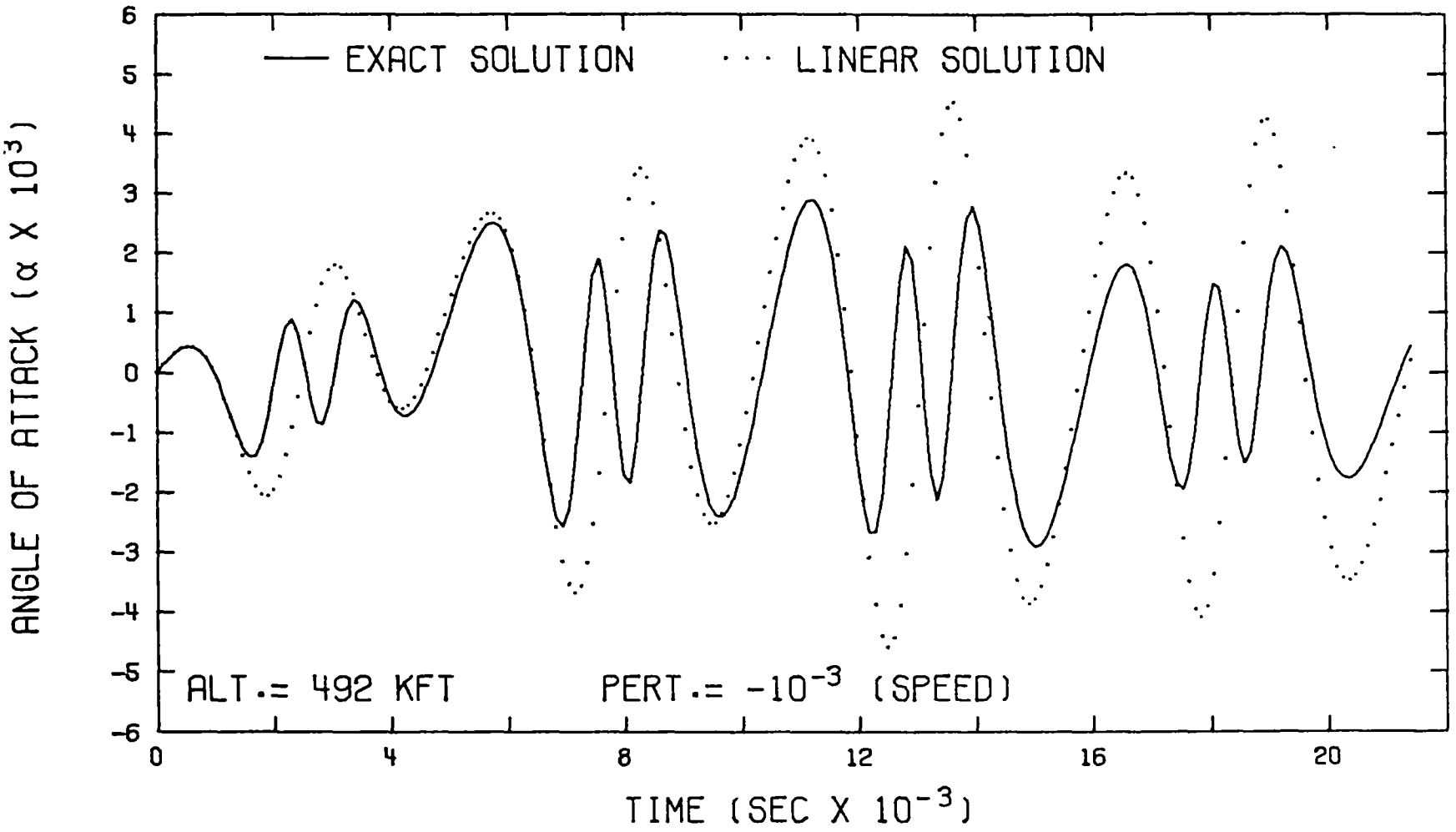

Fig. 18. Angle of attack vs time.

altitude the pitching motion is more complex, due to its nonlinearity. Figures 17 and 18 present the variations of radial distance and angle-of-attack as functions of time, The plots result from a numerical integration of the full set of nonlinear equations. Equations (6), at an altitude of 492000 ft, which is near the resonance altitude for the example vehicle with an initial nondimensional speed decrease of 10^{-3} ($\Delta\hat{u} = -10^{-3}$). The solid lines are obtained with the exact density law and the dotted lines present the time histories of the elements when a linear density law is used for the integration. As shown in Figure 17 the trajectory is nearly a Keplerian orbit with negligible effect due to the drag. Also it can be seen in Figure 18 the variations of angle-of-attack show the resonance effect with a slightly higher period. Also higher order atmosphere density gradients give more damping to the amplitude of oscillations. With these observations near the resonance altitude we need only consider the pitching mode variables while the trajectory variables r, V and γ are assumed known functions of the time. These are evaluated along the Keplerian orbit. Explicitly, if E is the eccentric anomaly which defines the position along the orbit, we have

$$\begin{aligned} r &= a(1 - \varepsilon \cos E) \\ \tan\gamma &= \frac{\varepsilon \sin E}{\sqrt{1-\varepsilon^2}} \\ V^2 &= \mu\left(\frac{2}{r} - \frac{1}{a}\right) \\ \sqrt{\frac{\mu}{a^3}}\, t &= E - \varepsilon \sin E \end{aligned} \tag{57}$$

where, a denotes the semimajor axis of the orbit, ε the eccentricity, and μ the gravitational constant. The time t is measured from the time of passage through perigee

and is related to the eccentric anomaly by means of the last equation, Kepler's equation. Although the trajectory variables are transcendental functions in time, if we restrict the analysis to nearly circular orbits these variables can be expressed as simple trigonometric functions through series expansions with respect to the eccentricity ε. The eccentricity is of the same order of magnitude as the non-dimensional perturbation in trajectory variables.

The pitching mode is governed by the system

$$\begin{aligned} \frac{\mathrm{d}q}{\mathrm{d}t} &= \frac{\varrho V^2 SLC_m(\alpha, q)}{2B} - \frac{3g(r)}{2r}\frac{(A-C)}{B}\sin 2\theta \\ \frac{\mathrm{d}\theta}{\mathrm{d}t} &= q + \frac{V}{r}\cos\gamma \end{aligned} \tag{58}$$

$$\theta = \gamma + \alpha .$$

From the last two equations we have

$$\frac{\mathrm{d}q}{\mathrm{d}t} = \frac{\mathrm{d}^2\gamma}{\mathrm{d}t^2} + \frac{\mathrm{d}^2\alpha}{\mathrm{d}t^2} + \frac{V}{r^2}\cos\gamma\frac{\mathrm{d}r}{\mathrm{d}t} + \frac{V}{r}\sin\gamma\frac{\mathrm{d}\gamma}{\mathrm{d}t} - \frac{1}{r}\cos\gamma\frac{\mathrm{d}V}{\mathrm{d}t}. \tag{59}$$

By substituting into the first equation and using Equations (1) to evaluate $\mathrm{d}r/\mathrm{d}t$, $\mathrm{d}V/\mathrm{d}t$, and $\mathrm{d}\gamma/\mathrm{d}t$ we have an equation in α.

$$\begin{aligned} &\frac{\mathrm{d}^2\alpha}{\mathrm{d}t^2} + \frac{T\cos\alpha}{mV}\frac{\mathrm{d}\alpha}{\mathrm{d}t} + \frac{\varrho SV}{2m}\frac{\mathrm{d}C_L(\alpha)}{\mathrm{d}t} + \frac{3g}{2r}\frac{(A-C)}{B}\cos 2\gamma\sin 2\alpha \\ &\quad + \frac{3g}{2r}\frac{(A-C)}{B}\sin 2\gamma\cos 2\alpha + \frac{T}{m}\frac{\varrho S}{2m}[C_L(\alpha)\cos\alpha + C_D(\alpha)\sin\alpha] \\ &\quad + \frac{T}{m}\frac{g}{V^2}(2\sin\gamma\sin\alpha + \cos\gamma\cos\alpha) - \left(\frac{T}{m}\right)^2\frac{\sin 2\alpha}{2V^2} \\ &\quad - \left(\frac{\varrho S}{2m}\right)^2 C_D(\alpha)\,C_L(\alpha)\,V^2 - \frac{\varrho SC_D(\alpha)}{2m}g\cos\gamma \\ &\quad - \frac{\varrho SV^2L}{2B}C_m(\alpha, q) + \frac{3g}{2r}\sin 2\gamma + \frac{SC_LV}{2m}\frac{\mathrm{d}\varrho}{\mathrm{d}t} - \frac{g^2}{V^2}\sin 2\gamma = 0. \end{aligned} \tag{60}$$

To get an analytical solution to the equation the following assumptions will be made:

(1) The lift coefficient varies linearly with the angle-of-attack while the drag coefficient remains nearly constant.

(2) The pitching moment coefficient is given approximately by

$$C_m = C_{m_\alpha}\sin\alpha\cos\alpha + \frac{L}{2u_0}C_{m_{\hat{q}}}\frac{\mathrm{d}\alpha}{\mathrm{d}t}. \tag{61}$$

The approximation applies to a slender vehicle with a conical surface of attack, and the stability derivatives C_{m_α} and C_{m_q} can be obtained from wind tunnel measurements or by using simple Newtonian impact theory for moderate angle-of-attack.

(3) The vehicle is moving along a slightly perturbed Keplerian ellipse about the reference circular orbit. Then

$$r = \frac{r_0(1-\varepsilon^2)}{1+\varepsilon\cos\tau} \tag{62}$$

where ε is small. To the order of magnitude of ε we have

$$\begin{aligned} r &= r_0(1-\varepsilon\cos\tau), & V^2 &= g_0 r_0(1+2\varepsilon\cos\tau) \\ V &= (g_0 r_0)^{1/2}(1+\varepsilon\cos\tau), & g &= g_0(1+2\varepsilon\cos\tau) \\ \sin\gamma &= \frac{\omega}{s}\varepsilon\sin\tau, & \cos\gamma &= \frac{\omega}{s}(1-2\varepsilon\cos\tau) \\ \varrho &= \varrho_0(1-\varepsilon\sigma_1\cos\tau), & \tau &= \frac{g_0\omega}{u_0}t. \end{aligned} \tag{63}$$

(4) To the order ε and near the resonance altitude, we neglect quantities of order η^2. With these assumptions, and using τ as a new independent variable, we have the quasilinear equation for the angle-of-attack.

$$\begin{aligned} &\alpha'' + \frac{\eta}{\omega}(C_{D_0} + C_{L_\alpha} - 2\delta C_{m_{\hat{q}}})\alpha' \\ &+ \frac{s^2}{\omega^2}[(3k_0 - 2\eta l\delta C_{m_\alpha}) - \varepsilon(3k_0 - 2\eta l\delta\sigma_1 C_{m_\alpha})\cos\tau]\sin\alpha\cos\alpha \\ &+ \frac{3\varepsilon s^2 k_0}{\omega^2}\sin\tau\cos 2\alpha = -\frac{\varepsilon s^2}{\omega^2}\left(1+\eta\frac{\omega}{s}\sigma_1 C_{L_0}\right)\sin\tau. \end{aligned} \tag{64}$$

A. NONLINEAR PITCHING FREQUENCY

As has been observed in Figure 18 the pitching motion computed numerically has a period slightly higher than the one predicted by the small perturbations equation. This is due to the effect of the initial perturbed angle-of-attack. The nonlinear frequency can be obtained from Equation (64) by neglecting the negligible damping and considering the oscillations along a circular orbit. Then we have

$$a'' + \left(\frac{n}{\omega}\right)^2 \sin\alpha\cos\alpha = 0. \tag{65}$$

Equation (65) can be integrated easily using the theory of elliptic integrals or the Lindstedt method for obtaining periodic solutions to nonlinear equations. The period of oscillation for large angle-of-attack obtained, in real time, is

$$P = \frac{2\pi u_0}{g_0 n}(1 + \tfrac{1}{4}\alpha_0^2 + \tfrac{1\,1}{1\,9\,2}\alpha_0^4 + \cdots) \tag{66}$$

where α_0 is the initial perturbed angle-of-attack.

B. ECCENTRICITY OSCILLATIONS

If the orbit is elliptical, the result for amplitude oscillations of the angle-of-attack is qualitatively different since some coefficients of the nonlinear equation are periodic quantities. The most significant effect is the forced oscillation due to the nonvanishing eccentricity of the orbit. This effect will give rise to a possibility of a resonance which may cause instability in the motion. To display the effect of the eccentricity oscillations, let us consider the case of small angle-of-attack. Equation (64) can be linearized to give

$$\alpha'' + \frac{2\eta C_{N_1}}{\omega}\alpha' + \left(\frac{n^2}{\omega^2} - \varepsilon b \cos\tau\right)\alpha = -\varepsilon c \sin\tau \tag{67}$$

where

$$\begin{aligned} b &= \frac{s^2}{\omega^2}(3k_0 - 2\eta l\delta\sigma_1 C_{m_\alpha}) \\ c &= \frac{s^2}{\omega^2}\left(1 + 3k_0 + \frac{\eta\omega}{s}\sigma_1 C_{L_0}\right). \end{aligned} \tag{68}$$

We notice that, along a circular orbit, $\varepsilon = 0$, and the equation reduces to a homogeneous linear equation with constant coefficients. To the order η its characteristic roots are given by

$$\lambda = -\frac{\eta C_{N_1}}{\omega} \pm i\frac{n}{\omega} \tag{69}$$

which is identical to the solution, Equation (46), to the order η. In this formulation we see that the linear pitching mode found in the preceding chapter is in fact the small oscillation of the vehicle along a circular orbit, and resonance effects cannot be observed. If the eccentricity of the orbit is taken into consideration, the equation governing the angle-of-attack, even in the linearized form, Equation (67), is a non-homogeneous equation with periodic coefficients and an approximate method has to be used to get its analytical solution.

We first consider the linear homogeneous equation.

$$\alpha'' + \frac{2\eta}{\omega}C_{N_1}\alpha' + \left(\frac{n^2}{\omega^2} - \varepsilon b \cos\tau\right)\alpha = 0. \tag{70}$$

To display the damping we use the Liouville transformation

$$\alpha = \exp\left(-\frac{\eta C_{N_1}}{\omega}\tau\right) w(\tau). \tag{71}$$

Then we have the new equation in w

$$w'' + \left(\frac{n^2}{\omega^2} - \varepsilon b \cos\tau\right) w = 0 \tag{72}$$

where a small constant of the order η^2 has been neglected in the coefficient of w.

The equation is a Mathieu equation and its solution can be obtained with classical methods. The homogeneous solution for α is a damped Mathieu solution, with negligible damping at high altitude. To this general solution we must add a particular solution of the non-homogeneous equation, Equation (67). For the example vehicle $c<0$ at all altitudes but it should be mentioned that for an arbitrary shaped satellite, aerodynamic and gravity forced oscillations may mutually cancel to the first order when we have

$$1 + 3k_0 + \eta\omega\sigma_1 C_{L_0} = 0\,. \tag{73}$$

To construct a particular solution we may neglect the small dissipative damping force and consider the equation

$$\alpha'' + \left(\frac{n^2}{\omega^2} - \varepsilon b \cos\tau\right)\alpha = -\varepsilon c \sin\tau\,. \tag{74}$$

Following Beletskii (1965) we assume a particular solution of the form

$$\alpha_e = -\varepsilon c \sin\tau\phi(\tau)\,. \tag{75}$$

By substituting into Equation (74) we have an equation for ϕ

$$(1 - x^2)\frac{\mathrm{d}^2\phi}{\mathrm{d}x^2} - 3x\frac{\mathrm{d}\phi}{\mathrm{d}x} + \left(\frac{n^2}{\omega^2} - 1 - \varepsilon b x\right)\phi = 1 \tag{76}$$

where

$$x = \cos\tau\,. \tag{77}$$

A particular solution of Equation (76) is sought as a series in terms of the small parameter ε. Let

$$\phi(x) = \phi_0 + \varepsilon\phi_1 + \varepsilon^2\phi_2 + \cdots\,. \tag{78}$$

Then by substituting into Equation (76) and equating terms of the same order of magnitude we have

$$\begin{aligned}
&(1 - x^2)\,\phi_0'' - 3x\phi_0' + \left(\frac{n^2}{\omega^2} - 1\right)\phi_0 = 1\\
&(1 - x^2)\,\phi_1'' - 3x\phi_1' + \left(\frac{n^2}{\omega^2} - 1\right)\phi_1 = bx\phi_0\\
&\cdots
\end{aligned} \tag{79}$$

where the prime here denotes differentiation with respect to $x=\cos\tau$. The system can be readily integrated to give

$$\begin{aligned}
\phi_0 &= \frac{\omega^2}{n^2 - \omega^2}\\
\phi_1 &= \frac{b\omega^4\cos\tau}{(n^2 - \omega^2)(n^2 - 4\omega^2)}, \cdots
\end{aligned} \tag{80}$$

and a particular solution of Equation (74) is

$$\alpha_e = -\frac{\varepsilon\omega^2 c}{(n^2-\omega^2)}\sin\tau - \frac{\varepsilon^2\omega^4 bc}{2(n^2-\omega^2)(n^2-4\omega^2)}\sin 2\tau\,. \tag{81}$$

Again we can see that $n^2=\omega^2$ corresponds to a resonance and at this altitude Equation (81) is meaningless because the linearization is not justified. Excluding the resonance altitude the correct solution for the angle-of-attack oscillations is the sum of the damped Mathieu solution, Equation (70) and the particular forced oscillation, Equation (81).

5. Conclusion

In this paper we have presented an analytical study of the longitudinal dynamics of a thrusting, lifting, orbital vehicle in a nearly circular orbit. Explicit expressions for the elements of the orbit were derived and the behaviors of the variations of these elements were correctly predicted. It was shown that, for large perturbations, the second order gradient effect of the air mass density must be included for an accurate analysis. Explicit expressions for the period and damping of the angle-of-attack mode were derived. A factorization of Etkin's stability quintic (Etkin, 1961) has been given and the values of the explicit roots obtained agree with the numerically computed roots up to five significant figures at all altitudes above 100000 ft, to within a few hundred feet below and above the resonance altitude. The resonance altitude where the two oscillatory modes have the same frequency can be obtained by solving a very simple equation. Resonance effect was displayed by a study of the forced eccentricity oscillations. It was shown that the small angle-of-attack oscillations of the vehicle along an orbit of small eccentricity are governed by a damped Mathieu equation with a periodic forcing term.

Acknowledgements

Suggestions by Professors Holt Ashley and Arthur E. Bryson, Jr. for the improvement of the original manuscript are gratefully acknowledged.

Notation

A, B, C = principal moments of inertia
a, b, c, d = numerical coefficients, Equation (52), Equation (68)
a = correctional factor, Equation (27), semi major axis, Equation (57)
C_D = drag coefficient
C_L = lift coefficient
C_m = pitching moment coefficient
C_{D_α}, C_{L_α}, C_{m_α}, $C_{m_{\hat{q}}}$ = stability derivatives
C_{N_1} = coefficient, Equation (10)

C_{N_2} = coefficient, Equation (10)
g = acceleration due to gravity
h_1 = correctional coefficient, Equation (39)
k_y = radius of gyration in pitch
k_0 = $(A-C)/B$
K = coupling coefficient, Equation (52)
L = mean chord, characteristic length
l = $2r_0/L$
m = mass of vehicle
n = angle-of-attack frequency
P = period
q = angular velocity in pitch relative to the Earth
$\hat{q}$ = $(L/2u_0)q$
r = radial distance from center of Earth
$\hat{r}$ = r/r_0
s = $\sqrt{u_0/g_0}\,r_0$, speed ratio
S = reference area
t = time
$\hat{t}$ = (g_0/u_0)t
$\hat{u}$ = V/u_0
T = thrust
u_0 = reference circular speed
w = transformation variable, Equation (71)
W = vehicle weight
V = speed along the orbit
X = vector state, Equation (12)
x = $\cos\tau$
α = angle-of-attack
β = density coefficient, Equation (10)
γ = flight path angle
δ = $(L/2k_y)^2$
ε = small perturbation, eccentricity of orbit
η = $\varrho_0 S u_0^2/2mg_0$
θ = angle of pitch
λ = characteristic value
μ = gravitational constant
ξ = density coefficient Equation (24)
ϱ = air mass density
σ = non-dimensional density gradients, Equation (9)
τ = $\omega\hat{t} = (\omega g_0/u_0)t$
ϕ = central range angle (Figure 1), function, Equation (75)
ω = phugoid frequency
ω_1 = phugoid frequency with drag correction.

Subscript

$( )_0$ = reference flight path

$( )_1$ = perturbed quantity

Appendix: Vehicle Characteristics

The characteristics of the vehicle geometry and the aerodynamic stability derivatives used in all numerical calculations are those used by Etkin (1961) and Rangi (1960) and are typical for a slender body, a cone or wedge of 3° semiangle. The values were derived from the simple Newtonian impact theory for moderate angles of attack. They are shown in Tables I and II.

TABLE I

Geometric and inertial parameters

$k_y = 6$ ft	$L = 50$ ft
$k_0 = -0.94$	$W/S = 30$ psf (sea level)

TABLE II

Aerodynamic stability derivatives

$C_{L_0} = 0.05$	$C_{D_0} = 0.0133$	$C_{m_{\hat{q}}} = \partial C_m/\partial((L/2u_0)q) = -0.028$
$C_{L_\alpha} = \partial C_L/\partial\alpha = 0.329$	$C_{D_\alpha} = \partial C_D/\partial\alpha = 0.15$	$C_{m_\alpha} = \partial C_m/\partial\alpha = -0.0548$

References

Beletskii, V. V.: 1966, *Motion of an Artificial Satellite About Its Center of Mass*, NASA Translation, NASA TTF-429.

Bellman, R.: 1964, *Perturbation Techniques in Mathematics, Physics, and Engineering*, Holt, Rinehart and Winston, Inc., New York, pp. 5–7.

Bogoliubov, N. N. and Mitropolsky, Y. A.: 1961, *Asymptotic Methods in the Theory of Non-Linear Oscillations*, Hindustan Publishing Corp., India.

Lancaster, O.E. (ed.): 1961, *High Speed Problems of Aircraft and Experimental Methods*, Vol. VIII in the series 'High Speed Aerodynamics and Jet Propulsion', Princeton University Press, Princeton, New Jersey, pp. 149–152.

Etkin, B.: 1960, 'Longitudinal Dynamics of a Lifting Vehicle in a Circular Orbit', UTIA Report No. 65, AFOSR TN-60-191.

Etkin, B.: 1961, 'Longitudinal Dynamics of a Lifting Vehicle in Orbital Flight', *J. Aerospace Sci.* **28**, 779–88.

Laitone, E. V. and Chou, Y. S.: 1965, 'Phugoid Oscillations at Hypersonic Speeds', *AIAA J.* **3**, 732–5.

Morth, R. and Speyer, J. L.: 1961, 'Divergence from Equilibrium Glide Path at Supersatellite Velocities', *Am. Rocket Soc.* **31**, 448–50.

Norman, W. S. and Meier, T. C.: 1963, 'Approximate Longitudinal Dynamics of a Lifting Orbital Vehicle', *AIAA Journal* **1**, 1662–3.

Porter, R. F.: 1961, 'The Linearized Long-Period Longitudinal Modes of Aerospace Vehicles in Equilibrium Flight', Air Force Flight Test Center, AFFTC-TN-61-2.
Rangi, R. S.: 1960, 'Non-Linear Effects in the Longitudinal Dynamics of a Lifting Vehicle in Orbital Flight', UTIA TN-40.
Roberson, R. E.: 1958, 'Gravitational Torque on a Satellite Vehicle', *J. Franklin Inst.* **265**, 13–22.
U.S. Standard Atmosphere: 1962, U.S. Government Printing Office, Washington, D.C.
U.S. Standard Atmosphere Supplements: 1966, U.S. Government Printing Office, Washington, D.C.